Chem, Volume *7*

Supplemental information

Single-molecule mechanics of synthetic aromatic amide helices: Ultrafast and robust non-dissipative winding

Floriane Devaux, Xuesong Li, Damien Sluysmans, Victor Maurizot, Evangelos Bakalis, Francesco Zerbetto, Ivan Huc, and Anne-Sophie Duwez

Table of contents

1 Supplementary figures

1.1 Synthetic scheme

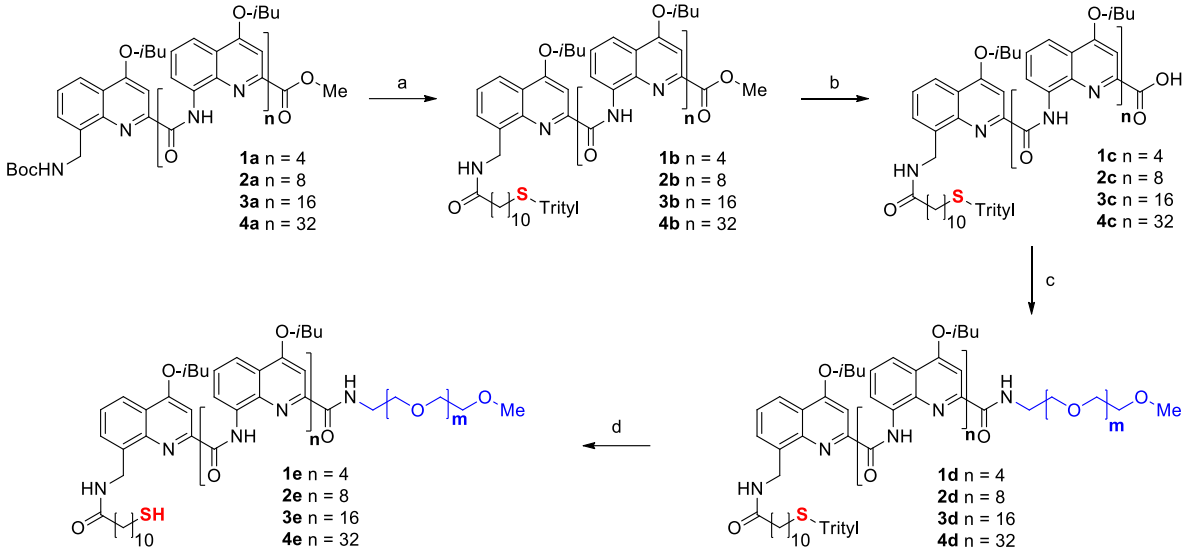

***Figure S1**: scheme of syntheses of targeted molecules functionalized with a thiol group and a PEG segment: a, i) TFA/DCM (1:1 vol/vol), rt, 3 h; ii) anchoring carboxylic acid, PyBOP, DIPEA, $CHCl_3$, 40 °C, overnight. b, NaOH, THF/MeOH (9:1 vol/vol), rt, 3 h. c, aminoPEG, PyBOP, DIPEA, $CHCl_3$, overnight. d, TFA/DCM/H_2O, rt, ~ 4 h.*

1.2 SMFS Data

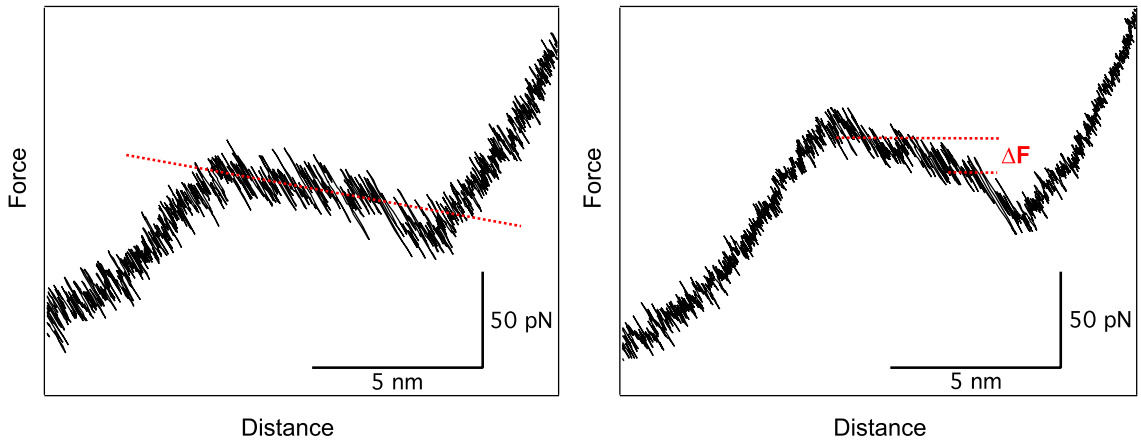

***Figure S2**: representative Force-Distance curves for pulling experiments on Q17 in DMF. The unwinding patterns show a tilted plateau, signature of the cooperativity. The amplitude of the tilt was estimated by measuring the force at the beginning and end of the plateau. The average ΔF (F end – F beginning) is –18 pN ± 0.6 pN.*

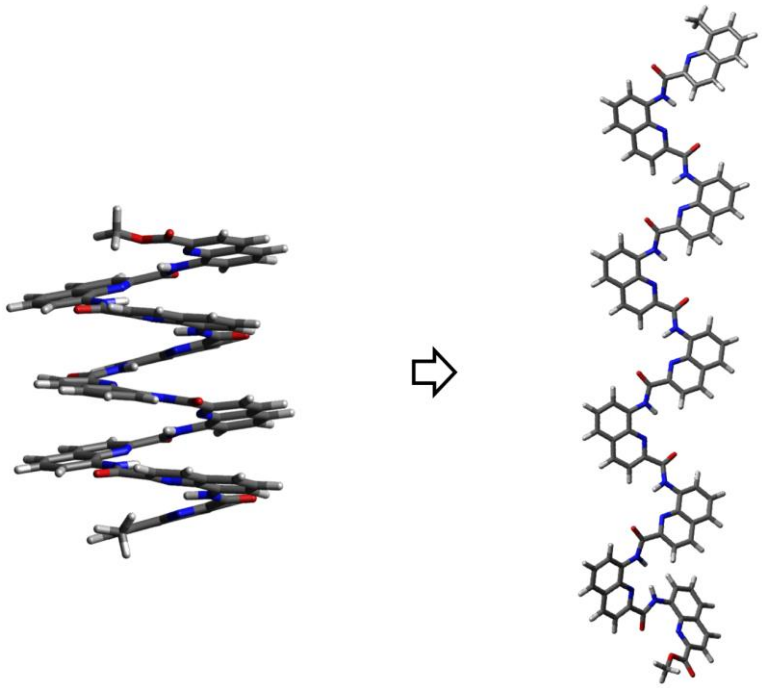

***Figure S3**: X-ray structure of Q9 and molecular model of the extended structure obtained by rotation of around 180° about each C−CO bond. The C−CO bond rotation is both the energetically least costly (see ref. 39 of the main text) and the one that leads to the largest chain extension, as opposed to the aryl-NH and amide bonds.*

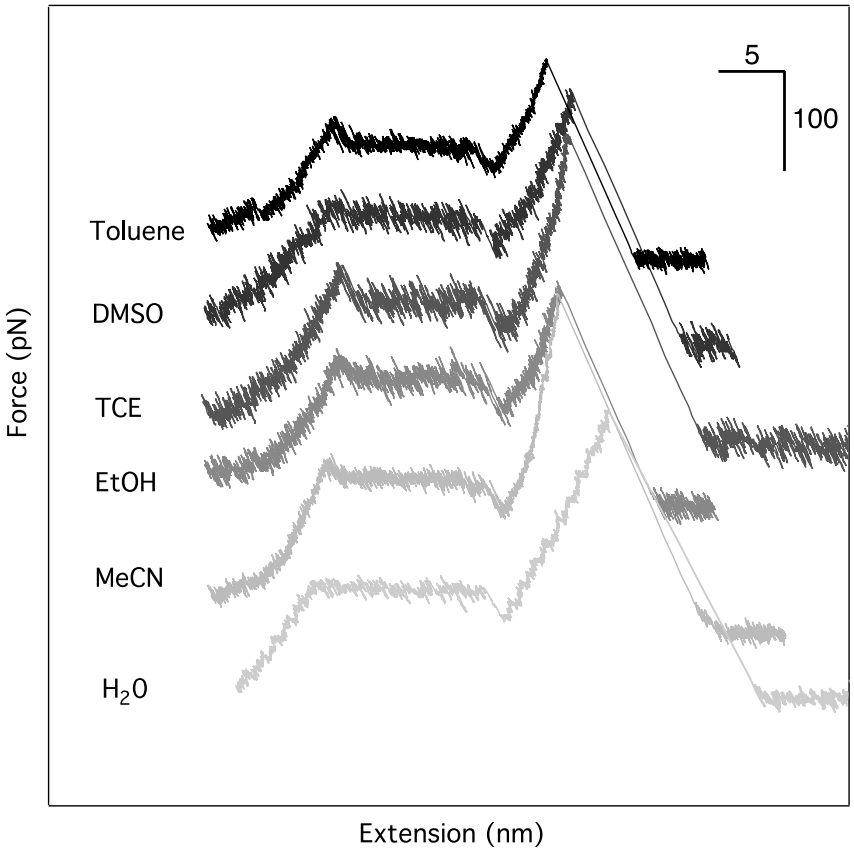

***Figure S4**: Force-distance curves of Q33 in various solvents: toluene, dimethylsulfoxide, tetrachloroethane, ethanol, acetonitrile, and water in physiological conditions (150 mM NaCl, pH7), all showing the same plateau length.*

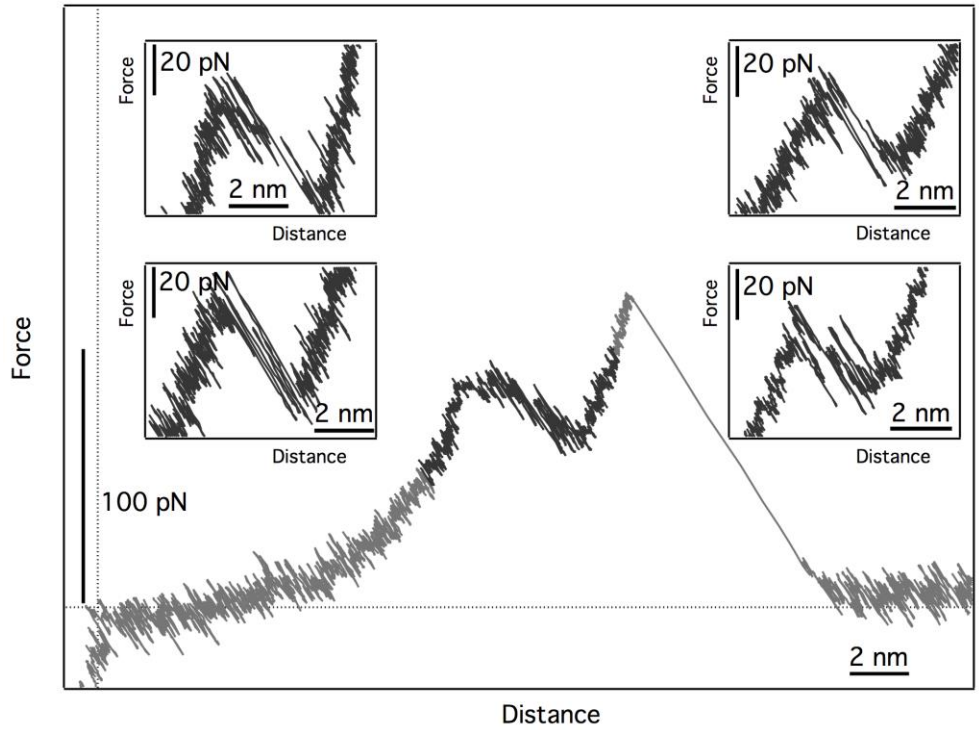

***Figure S5**: representative Force-Distance curves for pulling experiments on Q9 in DMF. The five curves can be sorted in 2 categories: first category (central curve) is analogue to the unwinding of Q33 and Q17 with a tilted plateau and some hopping events. In the second category (4 panels), the unwinding patterns show only large fluctuations.*

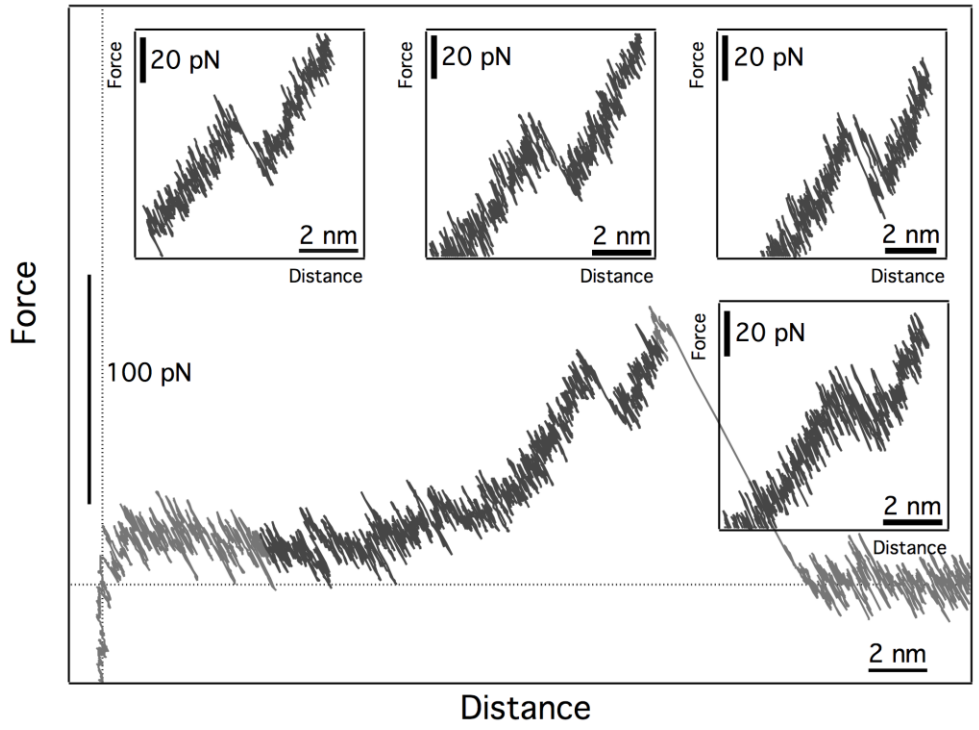

***Figure S6**: representative Force-Distance curves of pulling experiments on Q5 in DMF. The curves can be sorted in 2 categories: either a single peak or fluctuations.*

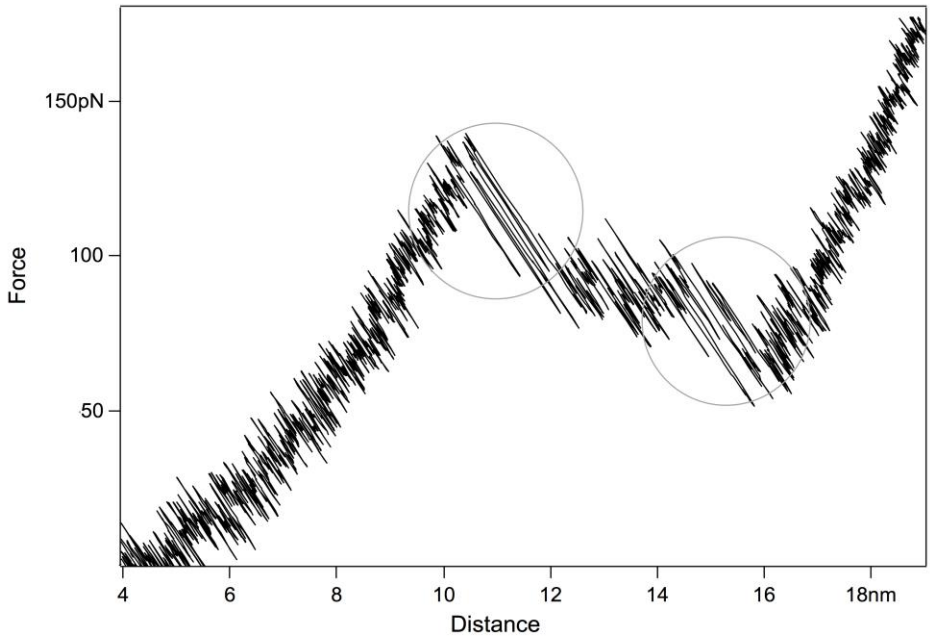

***Figure S7**: zoom in a representative Force-Distance curve of pulling experiments on Q17 in DMF. The curve shows large fluctuations at the beginning and end of the unwinding pattern.*

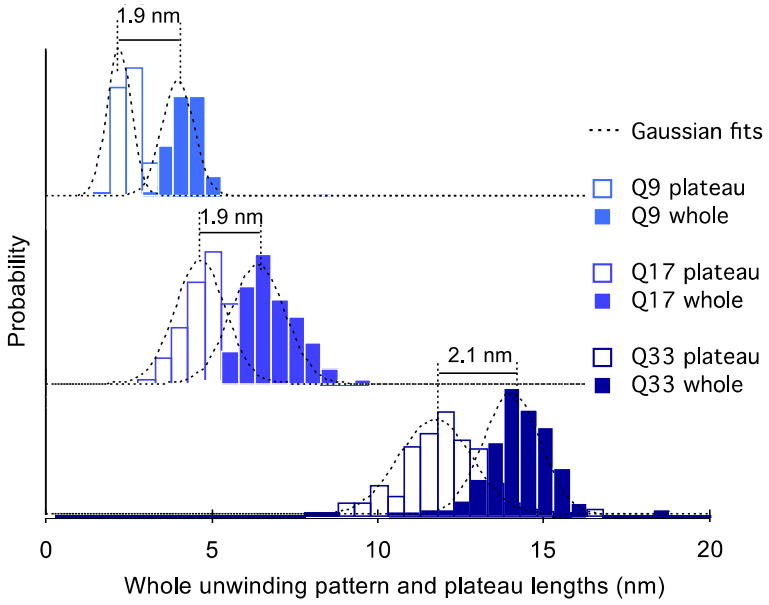

***Figure S8**: histograms of the lengths of the whole unwinding pattern and of the plateau for Q9, Q17, and Q33. The difference between the two lengths corresponds to the distance over which the fluctuations take place at the end of the plateau.*

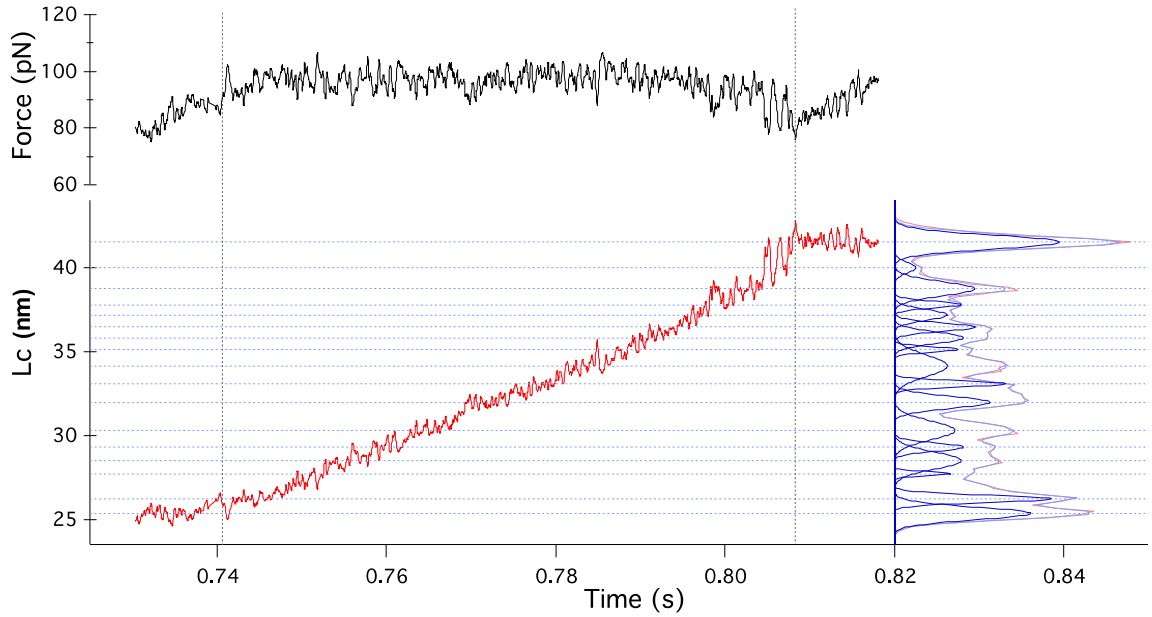

***Figure S9**: (Top) zoom in the helix unwinding area of force vs. time pulling curve of Q33. (Bottom left) The contour length evolution of the intermediate unwinding states represented as a function of time (red). (Bottom right) The corresponding contour length histogram (light red), the multi Gaussian peaks fitting the histogram (blue) and the overall fit trace (light blue). The dotted blue lines are the L_c values of the intermediate unwinding states (most probable values of the Gaussian fits).*

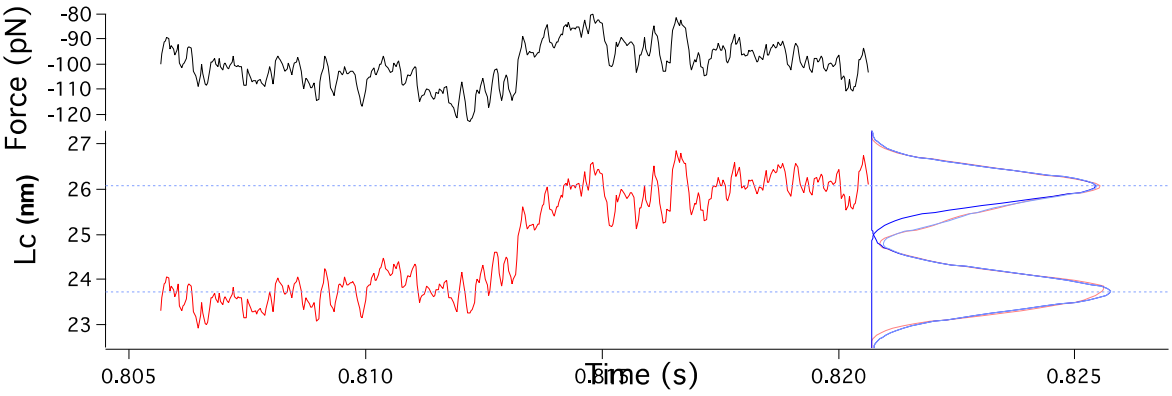

***Figure S10**: (Top) zoom in the helix unwinding area of Force vs. time pulling curve of the Q5, which exhibits only a single peak. (Bottom left) The contour length evolution of the intermediate unwinding states represented as a function of time (red). (Bottom right) The corresponding contour length histogram (light red), the multi Gaussian peaks fitting the histogram (blue) and the overall fit trace (light blue). The dotted blue lines are the L_c values of the intermediate unwinding states (most probable values of the Gaussian fits).*

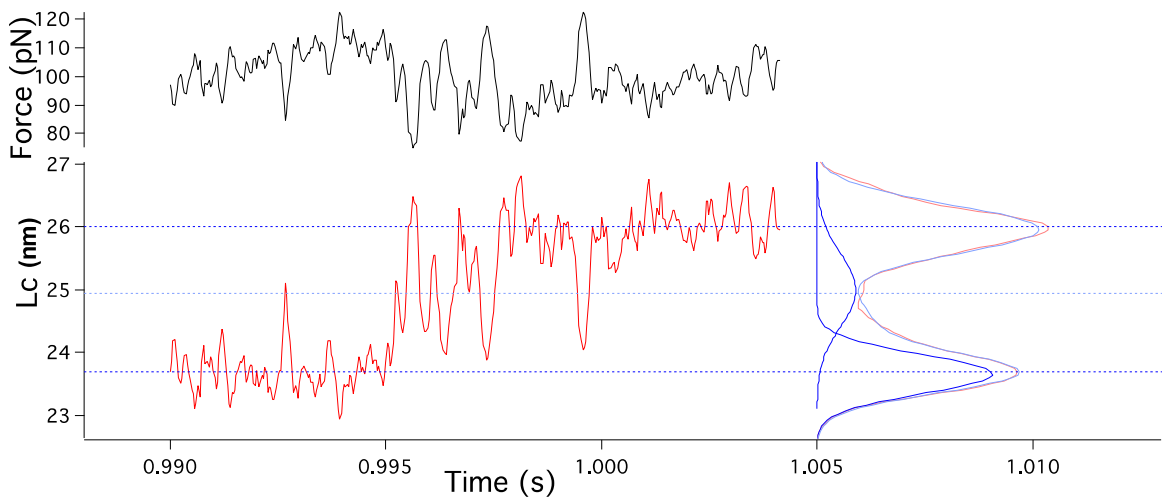

***Figure S11**: (Top) zoom in the helix unwinding area of Force vs. time pulling curve of Q5, which exhibits some fluctuations. (Bottom left) The contour length evolution of the intermediate unwinding states represented as a function of time (red). (Bottom right) The corresponding contour length histogram (light red), the multi Gaussian peaks fitting the histogram (blue) and the overall fit trace (light blue). The dotted blue lines are the L_c values of the intermediate unwinding states (most probable values of the Gaussian fits).*

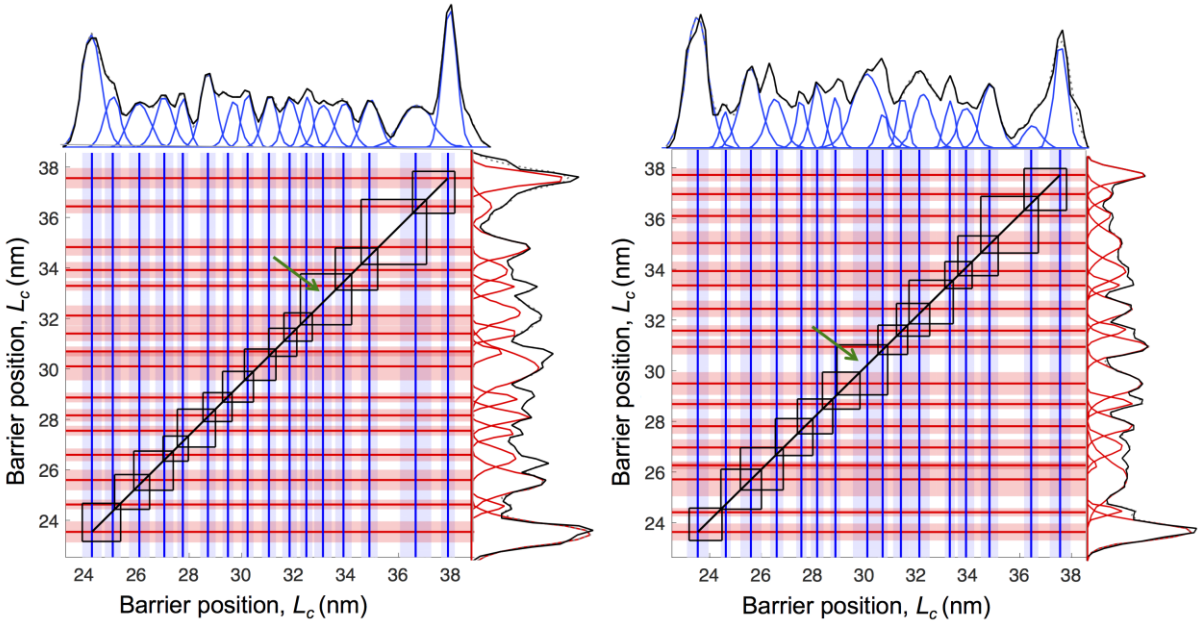

***Figure S12**: cross-superpositions of 2 histograms of L_c distributions for Q33. Red and blue lines represent the mean L_c values of the Gaussian fits of the L_c histograms with their 70% confidence interval (light red and light blue stripes). Diagonal rectangles are nearly always between 2 intermediate states. Green arrows: we observe 2 red lines and 3 blue lines, which means that there is a missing peak.*

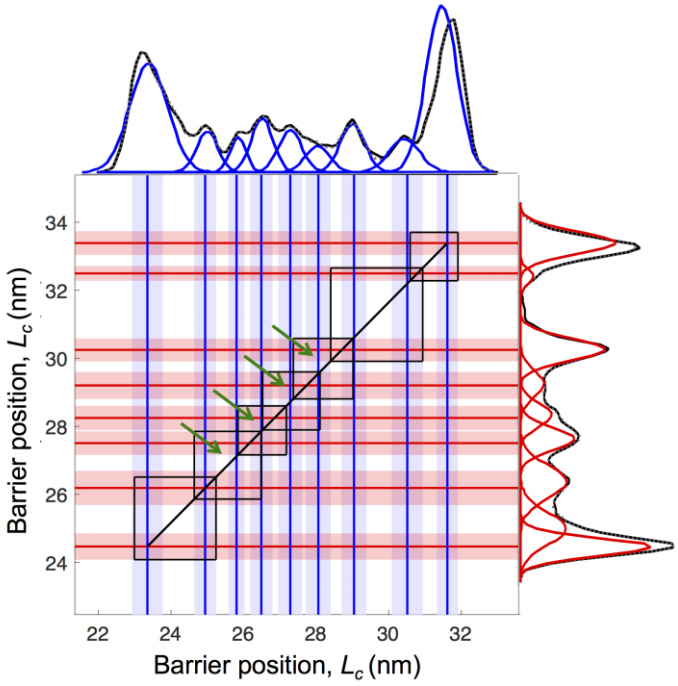

***Figure S13**: cross-superposition of 2 histograms of L_c distributions for Q17. Red and blue lines represent the mean L_c values of the Gaussian fits of the L_c histograms with their 70% confidence interval (light red and light blue stripes). The green arrows indicate missing peaks (in each rectangle, there are 3 blue lines for 2 red lines): the unwinding pathway is different in these two experiments.*

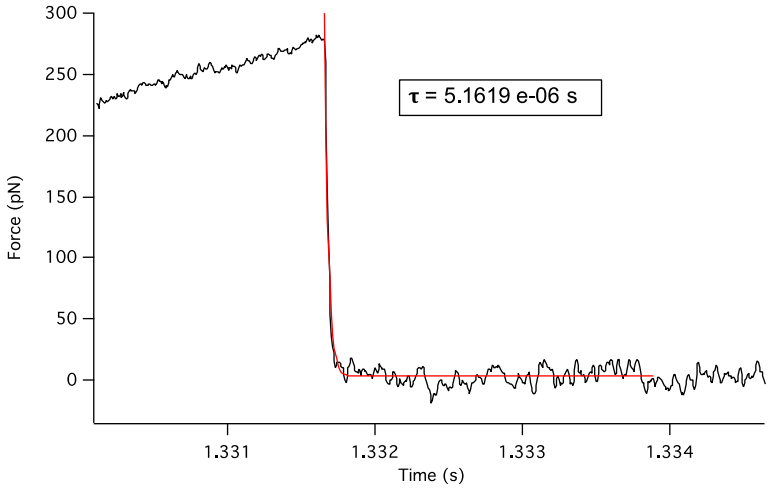

***Figure S14**: Force-versus-time curve detailing the response of the cantilever as the foldamer detaches from the tip. Data recorded at the highest pulling rate (4200 nm·s^{-1}). The response time (τ) was determined by an exponential fit (red line) to the curve.*

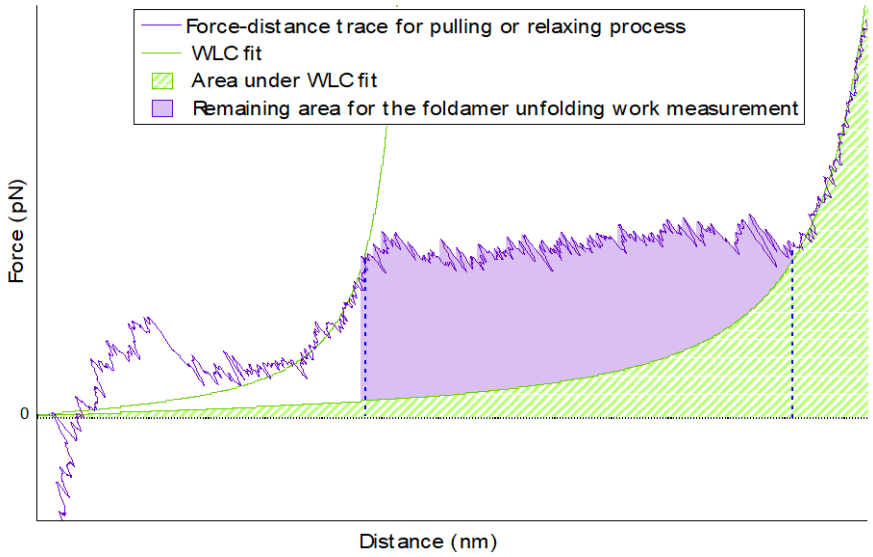

***Figure S15**: Illustration of the measurement of work in pulling-relaxing experiments. Force-distance curve observed during a pulling or relaxing experiment and WLC fits to remove the elastic contribution of the PEG linker. The purple shaded area corresponds to the work for the unfolding or the refolding process. It is measured by integrating the area under the pulling/relaxing curve and between the WLC fits.*

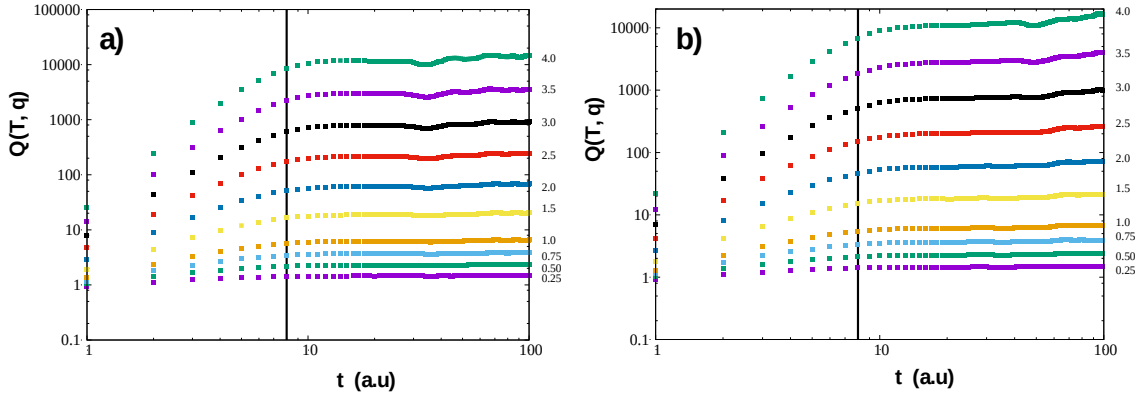

***Figure S16**: The moments, Q(t,q) as function of the lag time, t, for different values of the order of the moment, q: a) the moments for pulling process, and b) the moments for relaxing process. The estimated moments depicted in this figure use only data points form the plateau regime.*

1.3 NMR spectra of new compounds

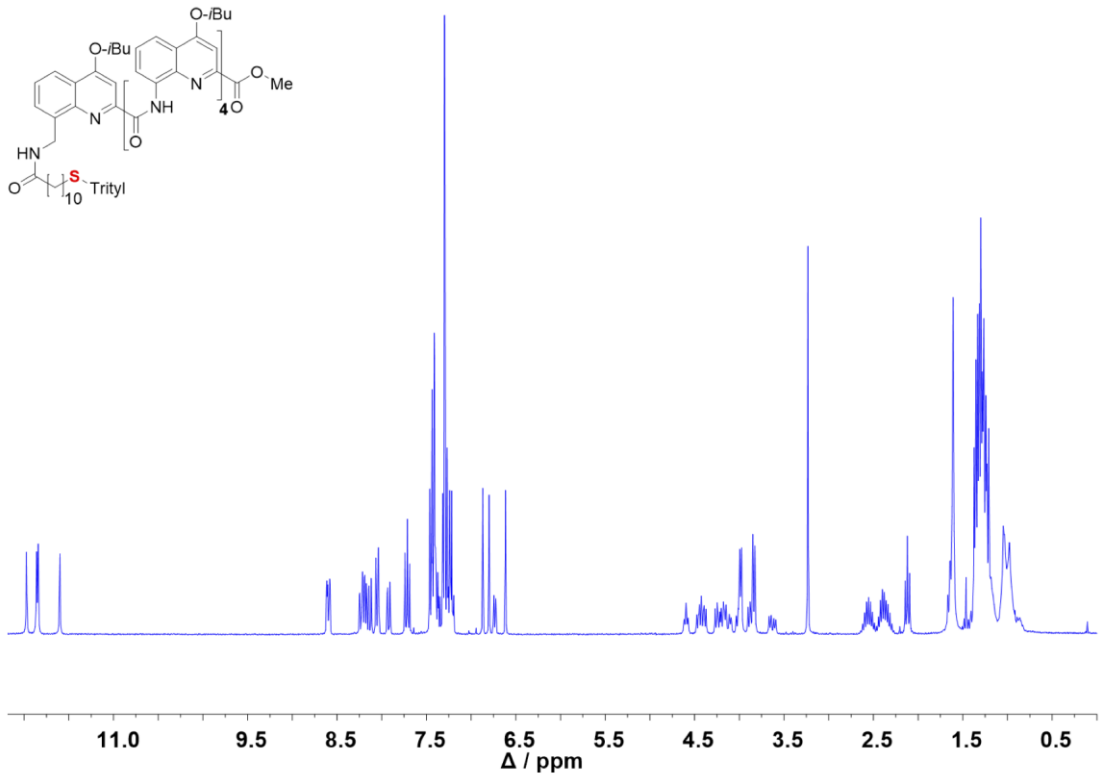

Figure S17. *[1]HNMR of* ***1b***

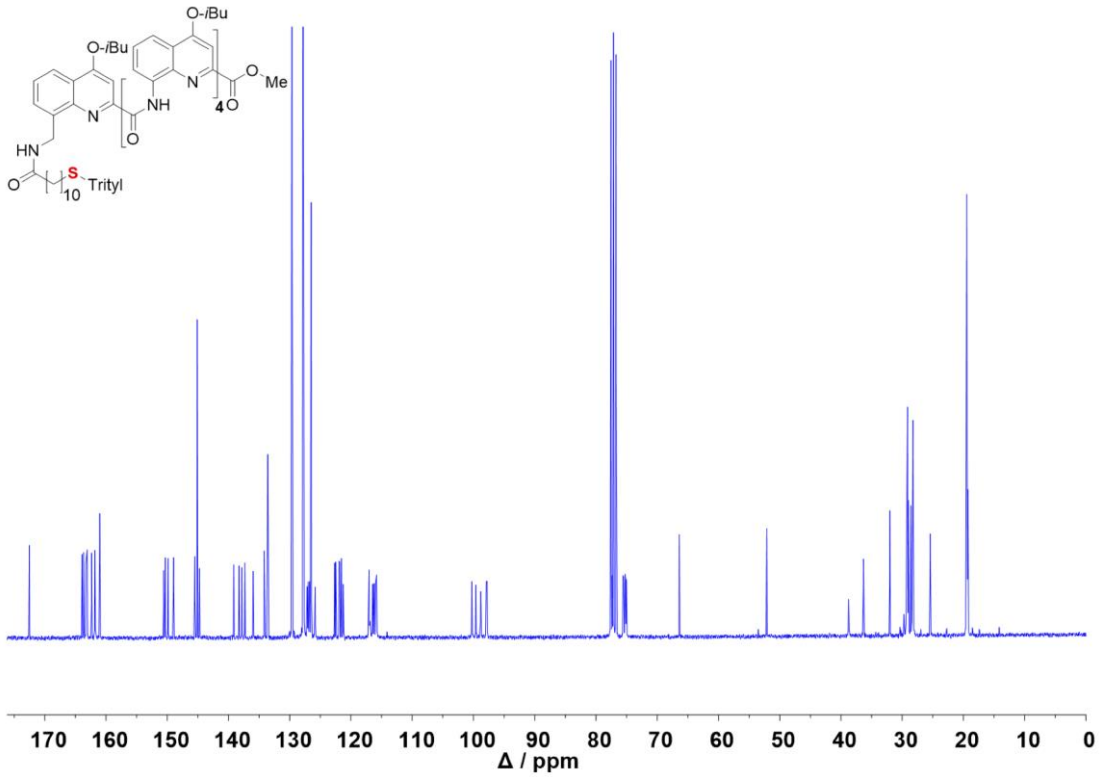

Figure S18. *[13]CNMR of* ***1b***

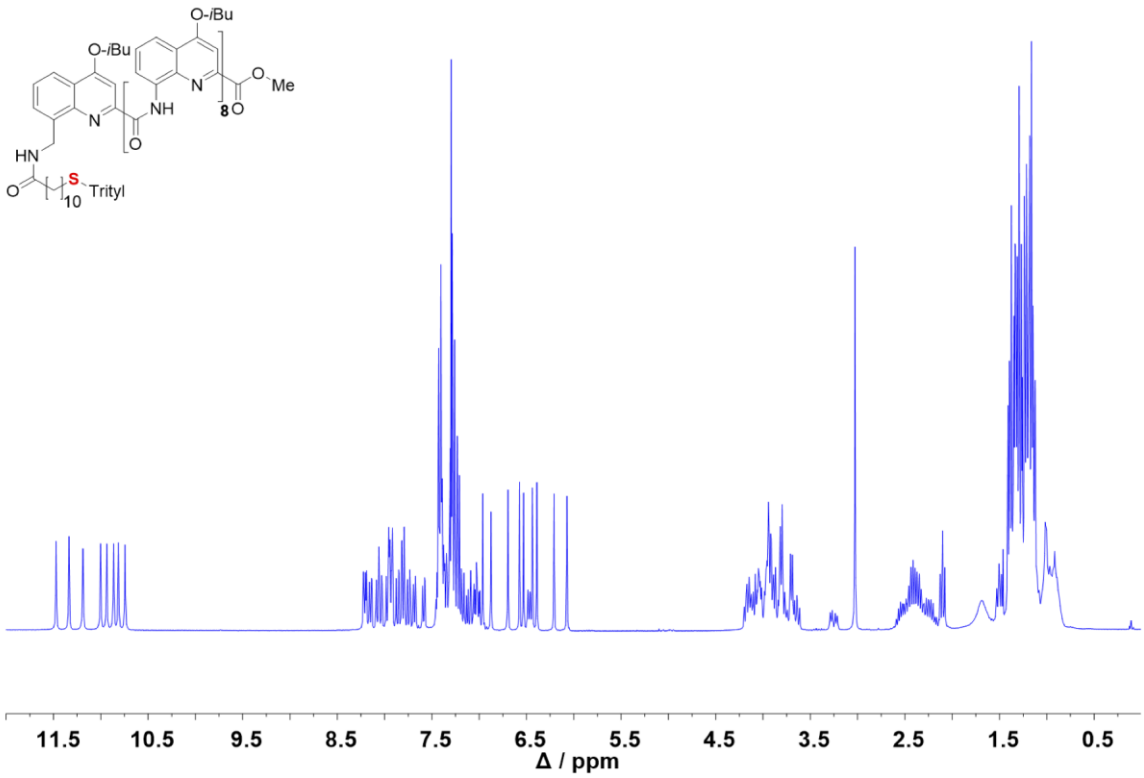

Figure S19. *[1]HNMR of* ***2b***

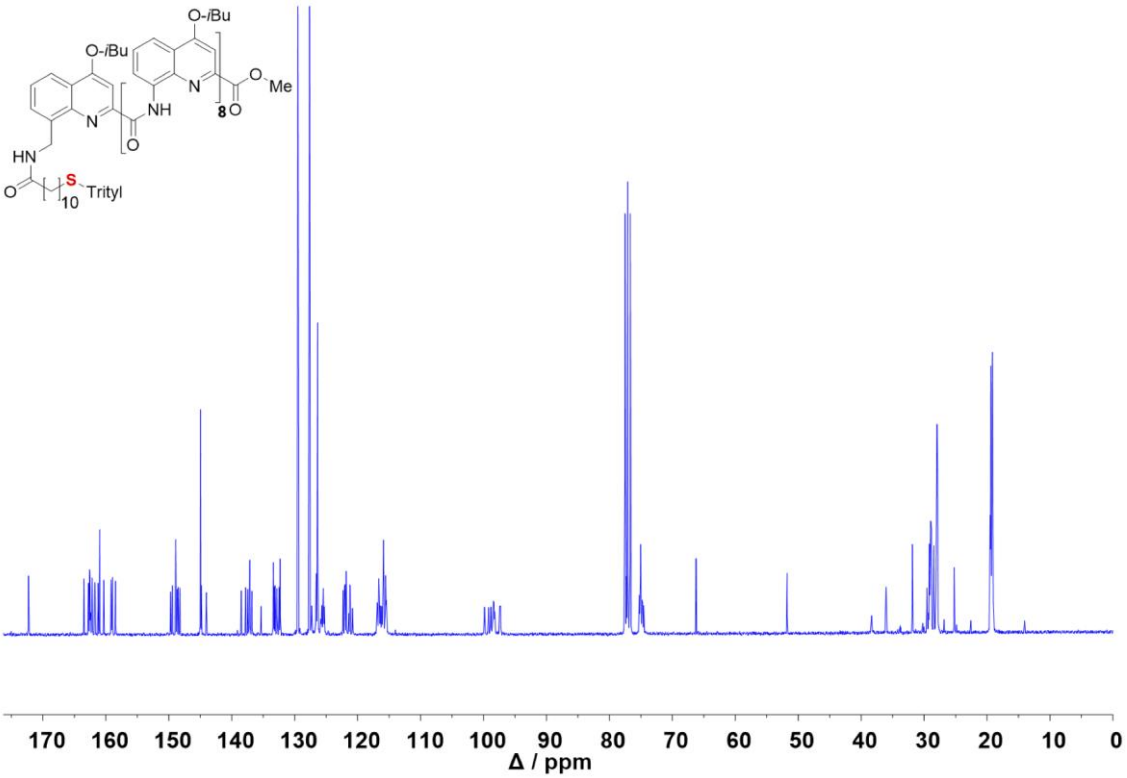

Figure S20. *[13]CNMR of* ***2b***

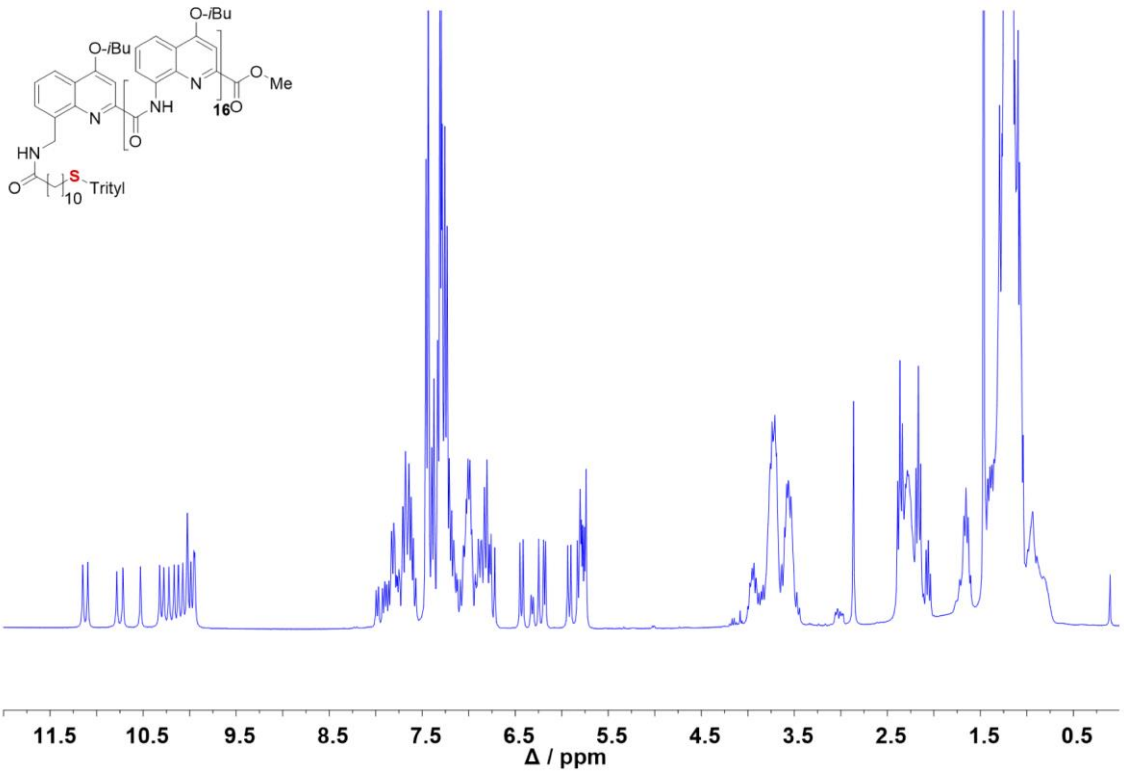

Figure S21. *^{1}HNMR of* ***3b***

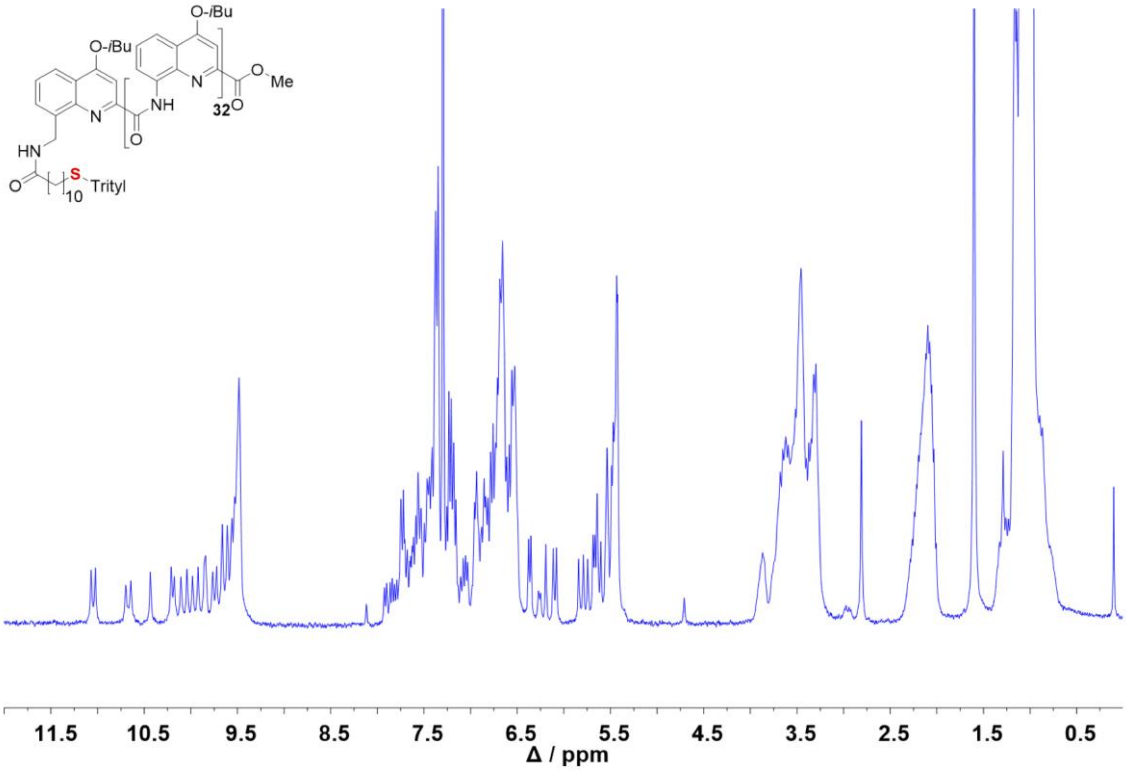

Figure S22. *^{1}HNMR of* ***4b***

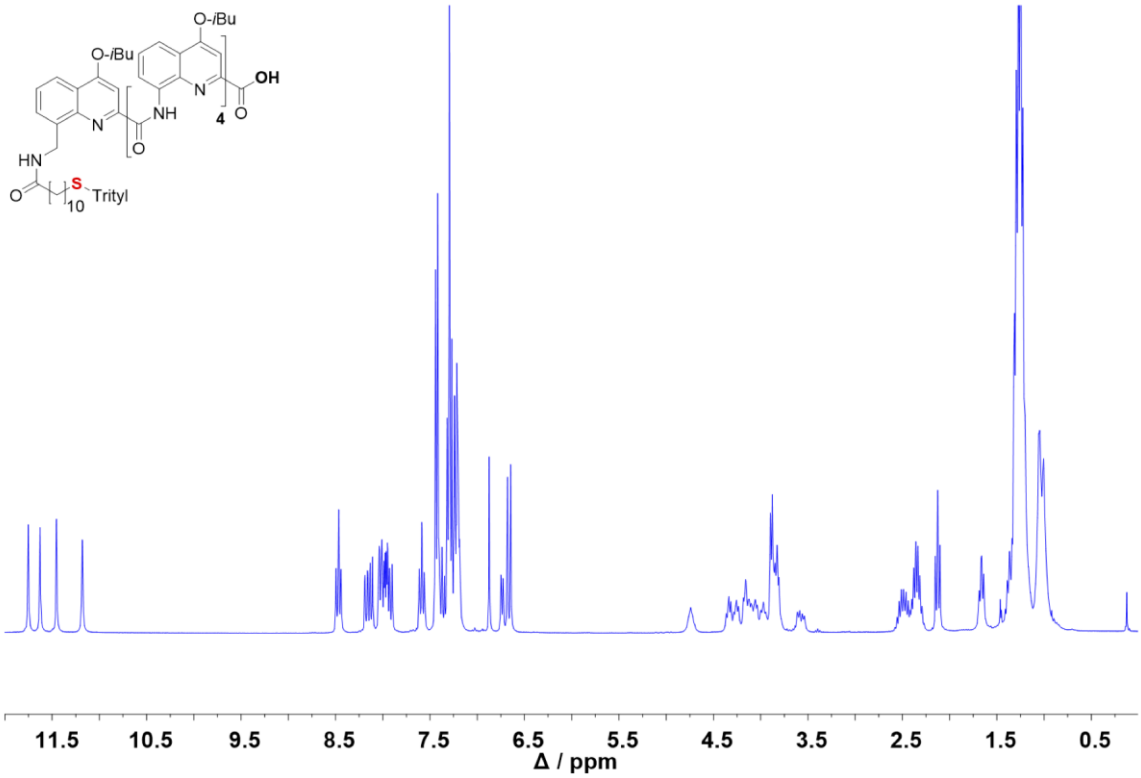

Figure S23. *^{1}HNMR of* ***1c***

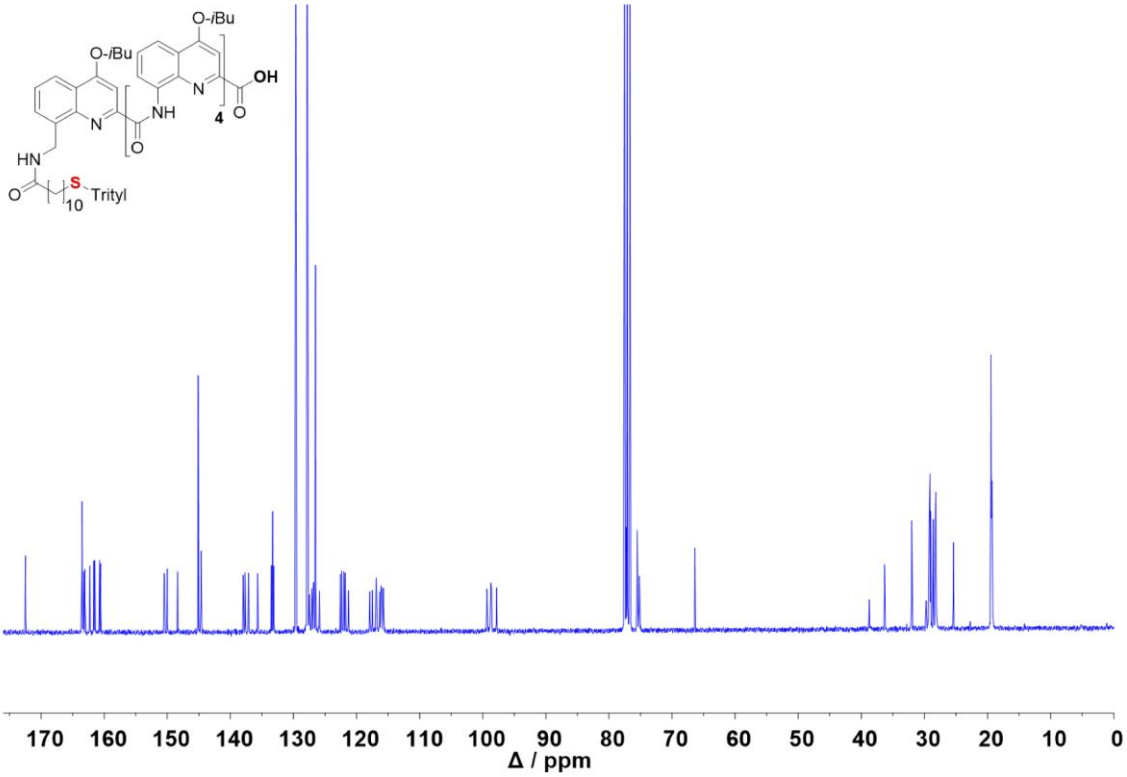

Figure S24. *^{13}CNMR of* ***1c***

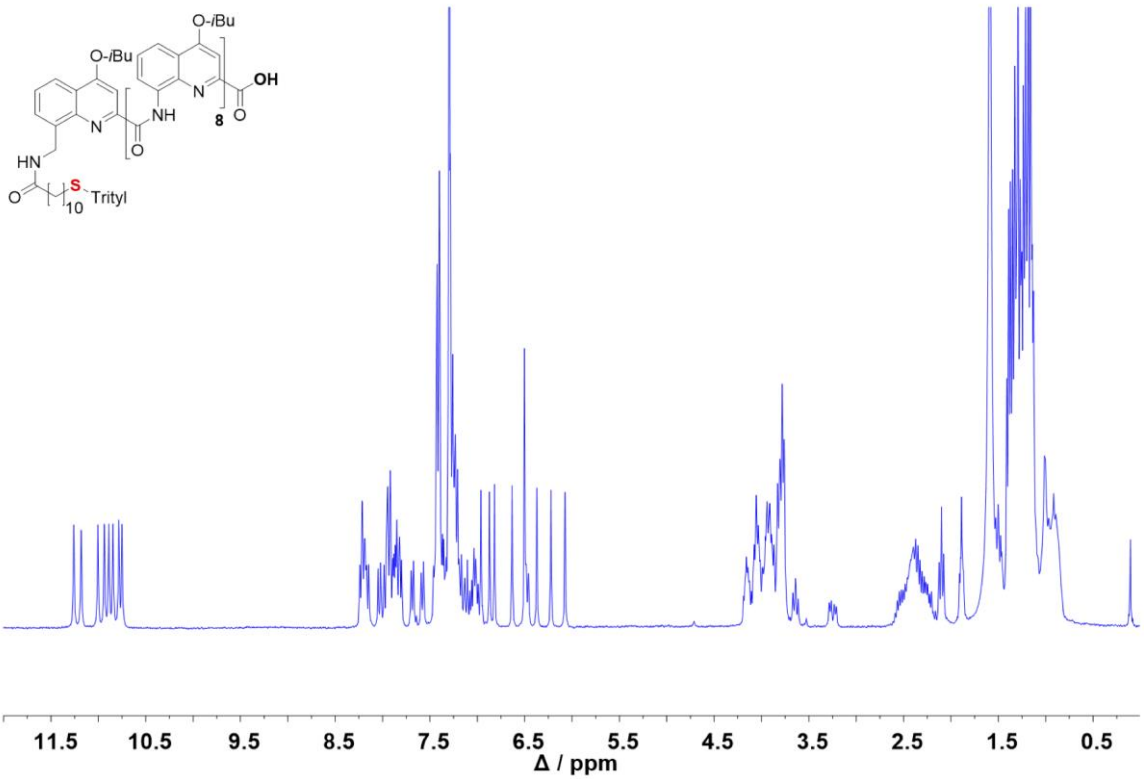

Figure S25. *[1]HNMR of* ***2c***

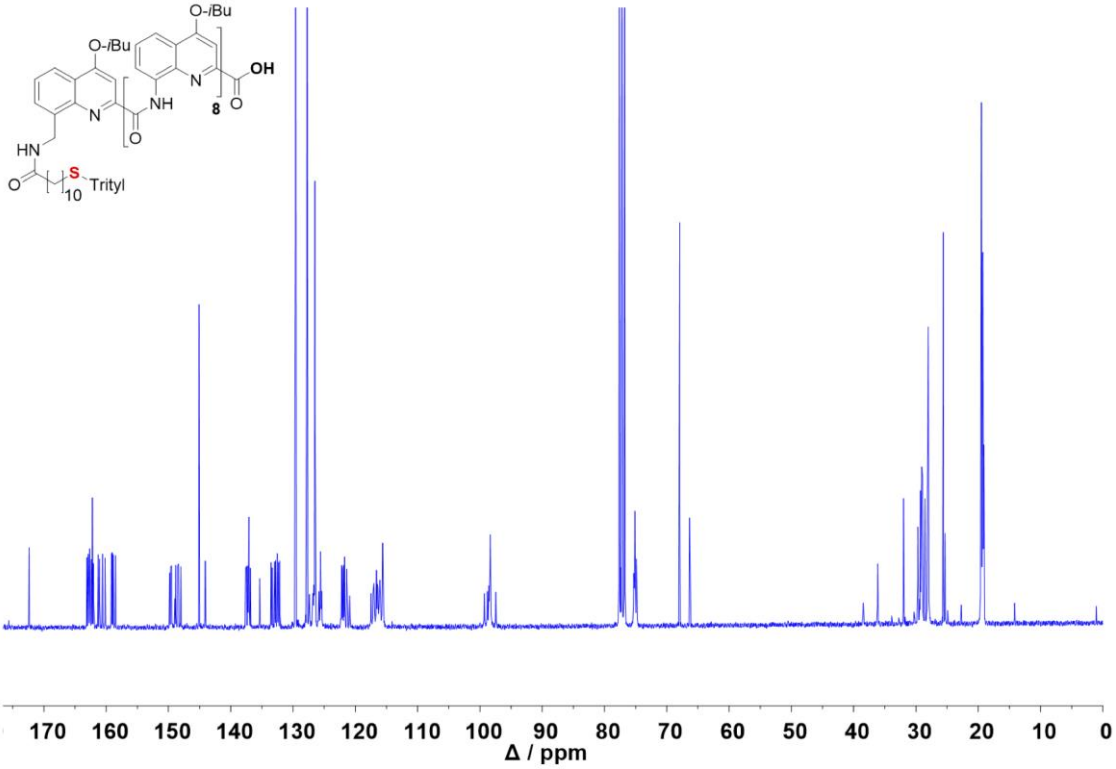

Figure S26. *[13]CNMR of* ***2c***

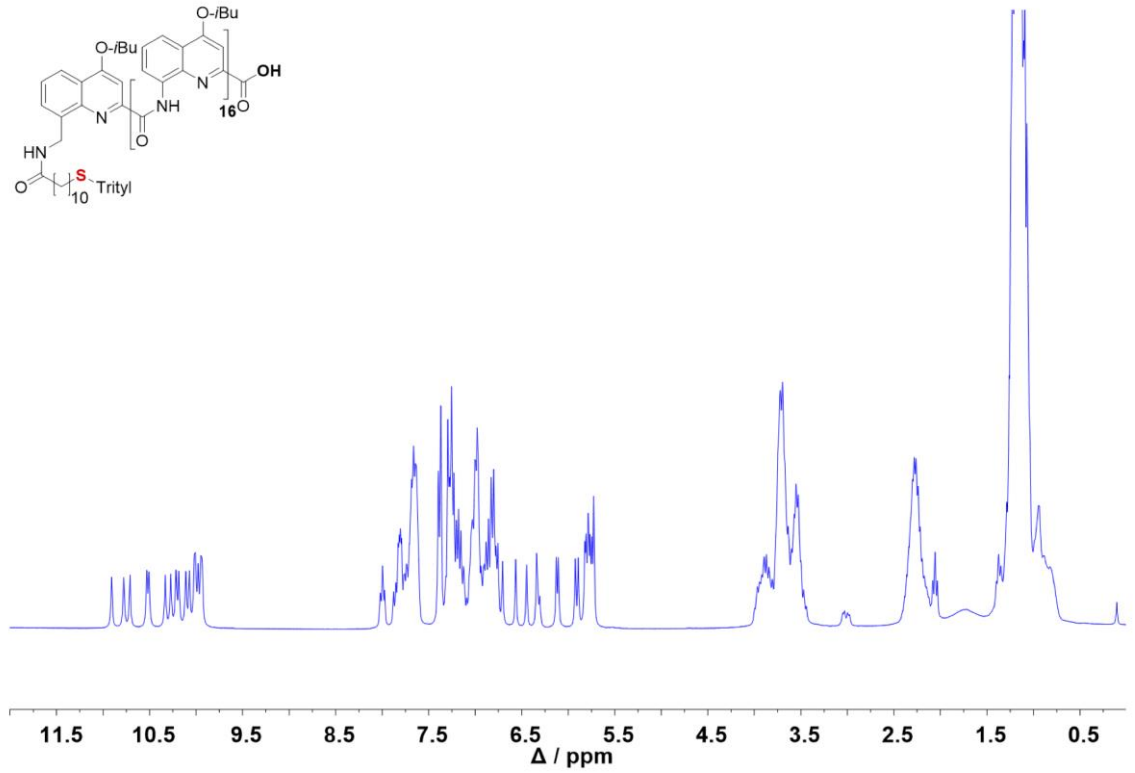

Figure S27. *[1]HNMR of* ***3c***

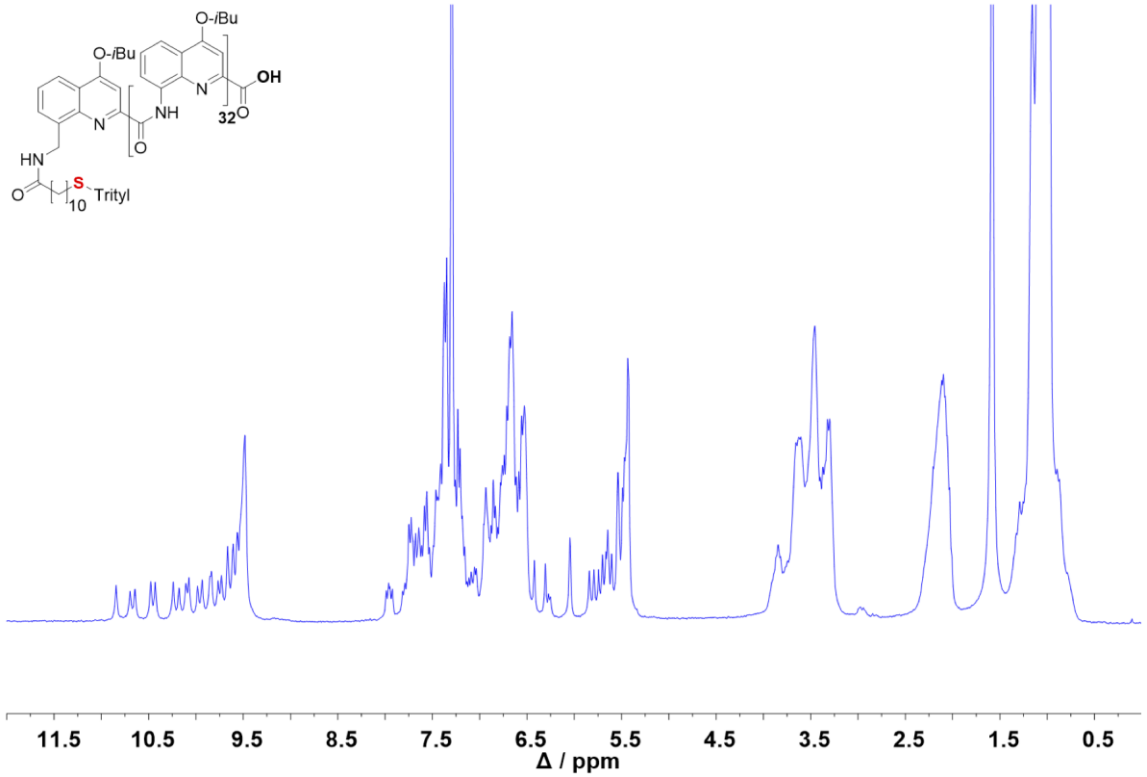

Figure S28. *[1]HNMR of* ***4c***

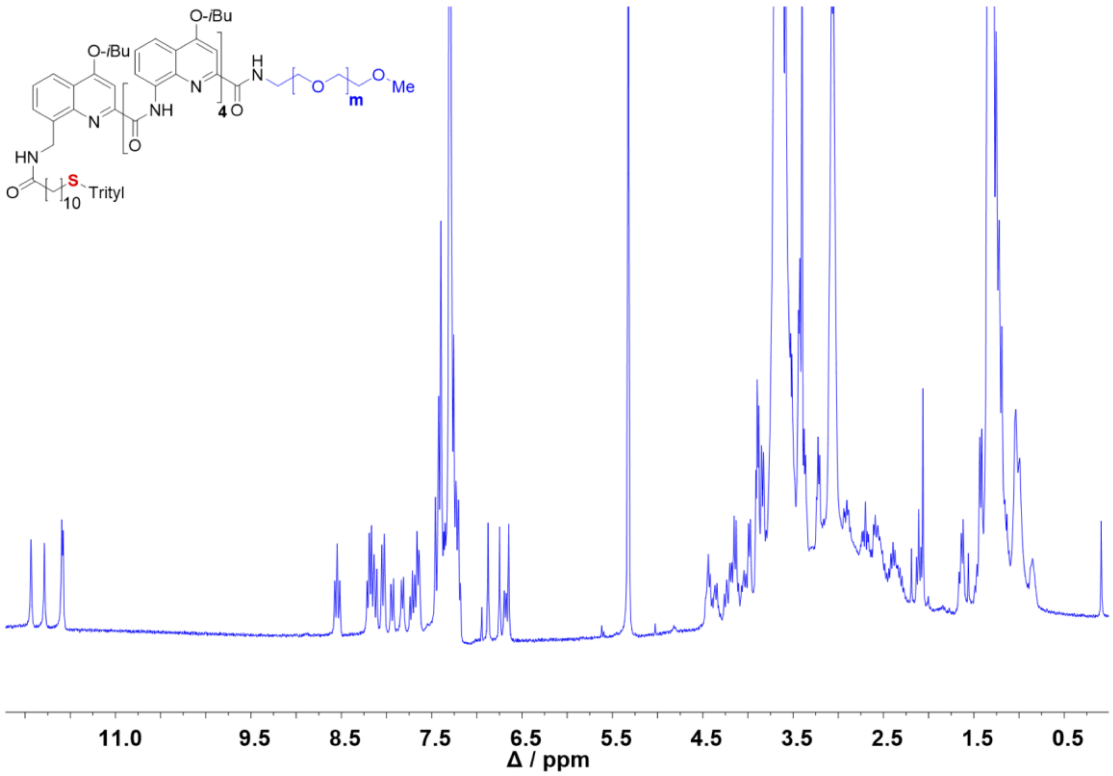

Figure S29. *^{1}HNMR of **1d***

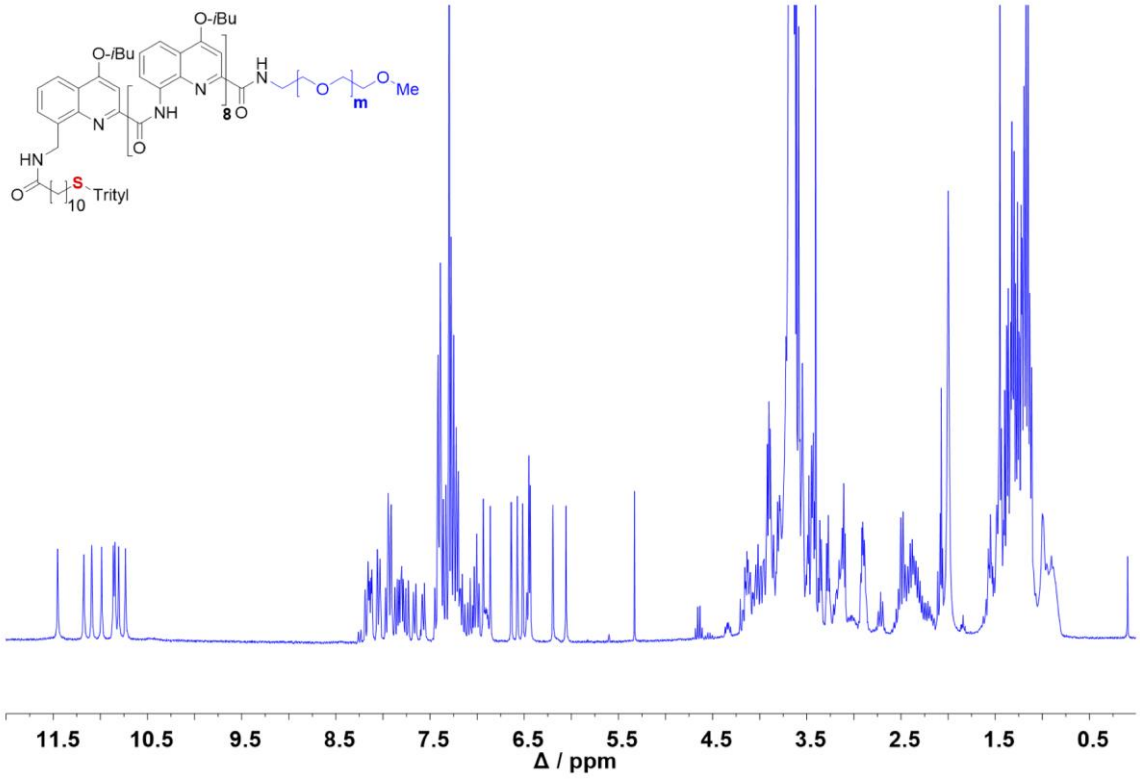

Figure S30. *^{1}HNMR of **2d***

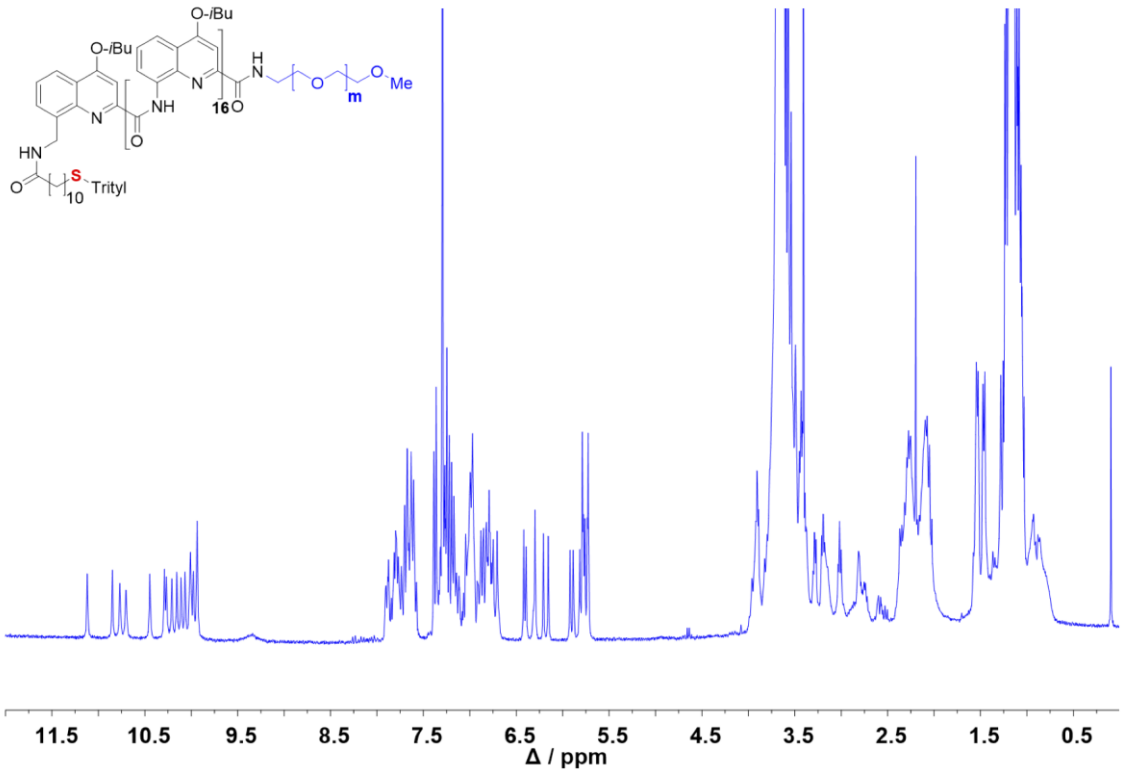

Figure S31. *[1]HNMR of* ***3d***

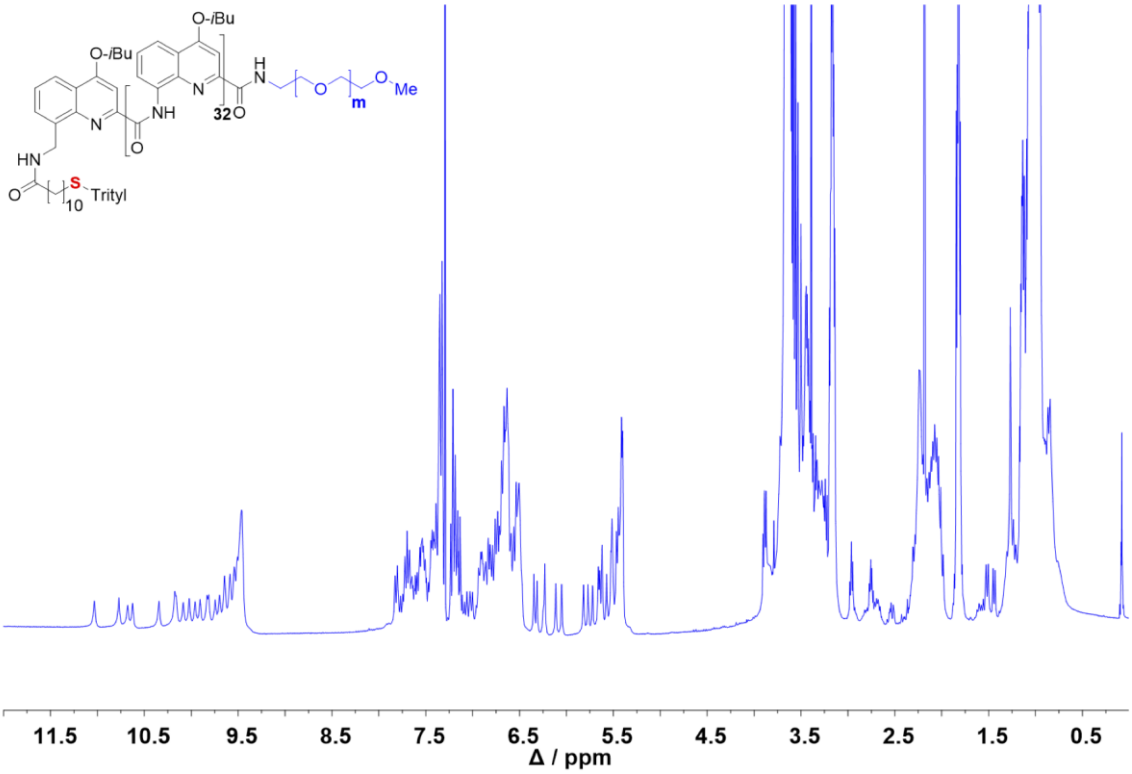

Figure S32. *[1]HNMR of* ***4d***

1.4 Supplementary Tables

***Table S1**. Structural parameters of helically folded and extended conformations of Q5-Q33.*

	Folded structure length (X-ray data) (0,14 nm/units) (nm)	Theoritical unfolded structure length (0,535 nm/units) (nm)	Theoritical length difference between unfolded and folded structures) (nm)	Experimental length of the unwinding plateau (nm)
Q5	0,7	2,675	1,975	1,9
Q9	1,26	4,815	3,555	3,4
Q17	2,38	9,095	6,715	6,5
Q33	4,62	17,655	13,035	13,9

***Table S2.** Parameters d and γ that deliver MSD for pulling and relaxing experiments for the plateau region.*

Regime	Pulling (msf(t)=dt^{γ})	Regime	Relaxing (msf(t)=dt^{γ})
[1:8]	d=5.069±0.679 γ=1.14±0.072	[1:8]	d=4.528±0.556 γ=1.14±0.066
[9:100]	d=47.085±1.085 γ=0.08±0.005	[9:100]	d=37.512±0.873 γ=0.141±0.006

***Table S3**. Parameters a and b obtained by fitting the moments of different order, for pulling/relaxing process, in the plateau regime.*

	Pulling				Relaxing			
q	[1:8]		[9:100]		[1:8]		[9:100]	
	a	b	a	b	a	b	a	b
0.25	0.986± 0.019	0.187± 0.012	1.405± 0.004	0.011± 0.001	0.960± 0.015	0.194± 0.010	1.369± 0.005	0.019± 0.001
0.50	1.117± 0.037	0.336± 0.020	2.125± 0.011	0.021± 0.001	1.072± 0.030	0.345± 0.017	2.013± 0.014	0.037± 0.002
0.75	1.316± 0.065	0.483± 0.029	3.338± 0.026	0.031± 0.002	1.245± 0.053	0.492± 0.025	3.069± 0.030	0.055± 0.002
1.0	1.613± 0.108	0.625± 0.036	5.413± 0.056	0.040± 0.003	1.506± 0.089	0.633± 0.034	4.828± 0.060	0.073± 0.003
1.5	2.697± 0.275	0.892± 0.056	15.349± 0.243	0.060± 0.004	2.459± 0.228	0.896± 0.051	12.903± 0.230	0.108± 0.004
2.0	5.069± 0.679	1.138± 0.072	47.085± 1.085	0.079± 0.005	4.528± 0.556	1.138± 0.066	37.512± 0.873	0.141± 0.006
2.5	10.427± 1.693	1.369± 0.085	153.505± 4.223	0.098± 0.007	9.124± 1.356	1.366± 0.079	116.77± 3.414	0.171± 0.007
3.0	22.993± 4.315	1.592± 0.098	526.173± 17.76	0.118± 0.008	19.720± 3.374	1.585± 0.089	385± 14	0.199± 0.009
3.5	53.614± 11.27	1.807± 0.109	1883.3± 76.2	0.138± 0.010	45.093± 8.635	1.799± 0.099	1334± 59	0.226± 0.011
4.0	130.671± 30.12	2.019± 0.118	7008± 336	0.157± 0.012	108.15± 22.8	2.010± 0.108	4832± 260	0.250± 0.013

***Table S4**. The analytical form of the structure function is illustrated for both pulling and relaxing experiments, when we consider only the plateau.*

Regime	Pulling	Regime	Relaxing
[1:8]	z(q)=hq-cqlog(q) h=0.627±0.002 c=0.088±0.002	[1:8]	z(q)=hq-cqlog(q) h=0.633±0.001 c=0.094±0.001
[9:100]	z(q)=hq h=0.039±0.0001	[9:100]	z(q)=hq-cq(q-1) h=0.074±2x10^{-4} c=0.004±1x10^{-4}

2 Supplementary methods

2.1 Resource availability

Lead Contact: Further information and requests for data and reagents should be directed to and will be fulfilled by the Lead Contact, Anne-Sophie Duwez (asduwez@uliege.be).
Materials availability: The new compounds generated in this study require substantial time and resources for their preparation. Samples may be provided upon request pending their availability. Any request for advice to perform their synthesis following the protocols reported below is welcome.
Data availability statement: The force curves supporting the current study have not been deposited in a public repository for lack of a standard data presentation, but are available from the Lead Contact on request.

2.2 Helices synthesis

2.2.1 Synthetic procedures

All anhydrous reactions were carried out using oven dried glassware and under a nitrogen atmosphere. All reagents bought from commercial sources were used as sold. Tetrahydrofuran (THF) and dichloromethane (DCM) were dried over alumina columns; anhydrous chloroform ($CHCl_3$), triethylamine (Et_3N) and diisopropylethylamine (DIPEA) were distilled over calcium hydride (CaH_2). Solvents were evaporated under reduced pressure using a Buchi rotary evaporator. Reactions were monitored by ^1H NMR by using a Bruker 300 MHz spectrometer and by thin layer chromatography (TLC) on Merck silica gel 60-F254 plates and observed under UV light (254 and 365 nm). Column chromatography was carried out on Merck GEDURAN Si60 (40-63 µm). Preparative recycling GPC (gel permeation chromatography) was performed on a set of 1H, 1.5H, 2.5H and 3H columns (JAIGEL 20×600 mm) JAIGEL 20*600 mm columns (Japan Analytical Industry) in chloroform/0.5~1% ethanol, as mobile phase, with a flow rate of 3.5 mL/min. The monitoring UV detector is UV-600 NEXT. High resolution mass spectra were obtained in the positive ion mode on a TOF spectrometer from the Mass Spectrometry Laboratory at the European Institute of Chemistry and Biology (UMS3033 & US001, IECB), Pessac, France. Starting materials, **1a**, **2a**, **3a** and **4a**, have been synthesized and reported in our previous publication.[1]

2.2.2 General procedure of syntheses of compound 1b, 2b, 3b and 4b

Compound **1a** (or **2a**, **3a** and **4a**) was stirred in TFA/chloroform (1:1 vol/vol) at room temperature for around 3 hours before azeotroping TFA with toluene *via* rotary evaporator. The resulting free amine was mixed with 11-(tritylthio)undecanoic acid, PyBOP and DIPEA in chloroform, reacting at 40 °C overnight. After evaporating the solvent, the residue was subjected to silica gel column to yield pure compound **1b** (**2b**, **3b** and **4b**).

2.2.2.1 Synthesis of 1b

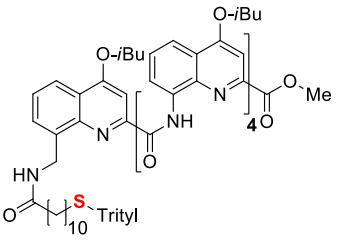

1a (190 mg, 0.140 mmol) was stirred with 50% TFA in $CHCl_3$ (3 mL) at room temperature around 3h. After that TFA was removed by azeotrope with toluene on rotary evaporator. Then crude amine was re-dissolved in dry $CHCl_3$ (4 mL), Trityl protected mercaptoundecanoic acid (161 mg, 0.35 mmol), PyBOP (182 mg, 0.35 mmol) and DIPEA (0.103 mL, 0.70 mmol) were added and the reaction mixture was stirred at 40 °C overnight. End product was purified with column chromatography by using 25% ethyl acetate in cyclohexane to give **1b** as a light yellow coloured solid (200 mg, 84%). ^1H NMR (300 MHz, $CDCl_3$): δ 11.97 (s, 1H), 11.86 (s, 1H), 11.84 (s, 1H), 11.60 (s, 1H), 8.61 (dd, 1H), 8.59 (dd, 1H), 8.25 – 8.11 (m, 4H), 8.06 (t, 1H), 8.03 (t, 3H), 7.92 (dd, 1H), 7.71 (t, 2H), 7.46 – 7.19 (m, 21H), 6.87 (s, 1H), 6.80 (s, 1H), 6.74 (d, 1H), 6.62 (s, 1H), 4.60 (t, 1H), 4.78 – 4.37 (m, 2H), 4.27 – 4.09 (m, 3H), 4.00 – 3.83 (m, 3H), 3.63 (dd, 1H), 3.23 (s, 3H), 2.64 – 2.27 (m, 5H), 2.12 (t, 2H), 1.64 (m, 2H), 1.37 –0.98 (m, 46H). ^{13}C-NMR ($CDCl_3$, 75 MHz): 172.53, 163.90, 163.65, 163.27, 163.13, 163, 07, 162.35, 161.83, 161.73, 161.03, 150.61, 150.32, 149.84, 148.97, 145.50, 145.11, 144.73, 139.12, 138.29, 137.83, 137.34, 135.97, 134.15, 133.59, 129.63, 127.80, 127.68,

127.14, 126.99, 126.76, 126.51, 125.85,122.67, 122.49, 121.93, 121.83, 121.56, 121.28, 117.10, 117.06, 116.92, 116.45, 116.22, 115.98, 115.85, 115.79, 100.28, 99.61, 98.82, 97.92, 97.76, 77.34, 75.59, 75.48, 75.22, 75.16, 75.04, 66.38, 52.12, 38.74, 36.33, 32.03, 29.33, 29.26, 29.21, 29.13, 29.02, 28.61, 28.36, 28.24, 28.22, 28.16, 25.42, 19.54, 19.46, 19.42, 19.36, 19.34, 19.28. MS (ES^+): *m/z* calcd for $C_{102}H_{111}N_{10}O_{12}S$ $[M+H]^+$ 1700.82, found 1700.81.

2.2.2.2 Synthesis of 2b

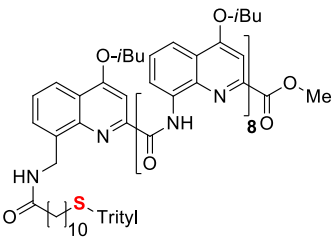

1b (250 mg, 0.107 mmol) was stirred with 25 % TFA in $CHCl_3$ (3 mL) at room temperature around 3h. After that TFA was removed by azeotrope with toluene on rotary evaporator. Then 155 mg of crude amine was re-dissolved in dry $CHCl_3$ (4 mL). Trityl protected mercaptoundecanoic acid (80 mg, 0.174 mmol), PyBOP (90 mg, 0.174 mmol) and DIPEA (0.05 mL, 0.345 mmol) were added and the reaction mixture was stirred at 40 °C overnight. End product was purified by column with 25% ethyl acetate in cyclohexane to give **2b** as a light yellow coloured solid (169 mg, 91 %). ^{1}H NMR (300 MHz, $CDCl_3$): δ 11.47 (s, 1H), 11.34 (s, 1H), 11.19 (s, 1H), 11.00 (s, 1H), 10.94 (s, 1H), 10.86 (s, 1H), 10.81 (s, 1H), 10.74 (s, 1H), 8.22 (dd, 1H), 8.20 (dd, 1H), 8.15 (dd, 1H), 8.060 (t, 1H), 8.059 (dd, 1H), 7.99 –7.92 (m, 4H), 7.86 (dd, 1H), 7.82 (d, 1H), 7.79 (d, 1H), 7.75 (dd, 1H), 7.68 (dd, 1H), 7.59 (dd, 1H), 7.46 – 6.99 (m, 27H), 6.96 (s, 1H), 6.87 (s, 1H), 6.70 (s, 1H), 6.57 (s, 1H), 6.53 (s, 1H), 6.47 (s, 1H), 6.44 (s, 1H), 6.39 (s, 1H), 6.21 (s, 1H), 6.07 (s, 1H), 4.20 – 3.61 (m, 18H), 3.25 (dd, 1H), 3.03 (s, 3H), 2.59 – 2.14 (m, 9H), 2.10 (t, 2H), 1.51 (t, 2H), 1.41 – 0.92 (m, 70H). ^{13}C-NMR ($CDCl_3$, 75 MHz): 172.29, 163.51, 162.77, 162.61, 162.58, 162.54, 162.47, 162.41, 162.17, 162.13, 161.74, 161.23, 160.97, 160.35, 159.17, 159.03, 158.95, 158.45, 149.71, 149.44, 148.91, 148.87, 148.69, 148.50, 148.23, 144.97, 144.84, 144.05, 138.48, 137.79, 137.44, 137.21, 137.18, 137.14, 136.79, 135.32, 133.40, 133.26, 133.11, 132.81, 132.46, 132.32, 129.48, 127.66, 127.29, 126.58, 126.37, 125.82, 125.69, 125.47, 125.31, 122.32, 122.09, 122.02, 121.96, 121.83, 121.37, 121.23, 121.17, 120.83, 116.90, 116.83, 116.62, 116.55, 116.39, 116.17, 115.90, 115.56, 115.43, 99.85, 99.20, 98.83, 98.52, 98.44, 98.34, 98.24, 97.44, 97.23, 77.30, 75.25, 75.16, 75.04, 74.80, 74.73, 74.55, 66.24, 51.77, 38.34, 36.04, 31.87, 29.58, 29.28, 29.25, 29.16, 29.07, 29.01, 28.95, 28.91, 28.85, 28.45, 28.09, 28.05, 28.01, 27.96, 27.92, 27.86, 26.81, 25.23, 22.58, 19.50, 19.48, 19.43, 19.41, 19.38, 19.35, 19.28, 19.19, 19.16, 19.07, 19.03, 14.04. MS (ES^+): *m/z* calcd for $C_{158}H_{167}N_{18}O_{20}S$ $[M+H]^+$ 2669.23, found 2669.23.

2.2.2.3 Synthesis of 3b

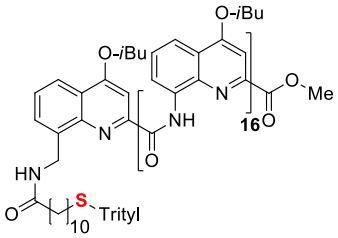

3a (75 mg, 0.017 mmol) was stirred with 50 % TFA in $CHCl_3$ (2 mL) at room temperature around 3h. After that TFA was removed by azeotrope with toluene on rotary evaporator. Then crude amine was re-dissolved in dry $CHCl_3$ (3 mL). Trityl protected mercaptoundecanoic acid (20.7 mg, 0.045 mmol), PyBOP (23.4 mg, 0.045 mmol) and DIPEA (0.013 mL, 0.09 mmol) were added and the reaction mixture was stirred at 40 °C overnight. End product was purified by precipitated in MeOH to give **3b** as a light yellow coloured solid (74 mg, 91 %). ^{1}H NMR (300 MHz, $CDCl_3$): δ 11.15 (s, 1H), 11.10 (s, 1H), 10.78 (s, 1H), 10.72 (s, 1H), 10.53 (s, 1H), 10.32 (s, 1H), 10.28(s, 1H), 10.22 (s, 1H), 10.17 (s, 1H), 10.12 (s, 1H), 10.07 (s, 1H), 10.03 (s, 2H), 9.99 (s, 1H), 9.95 (s, 1H), 9.94 (s, 1H), 7.98 (d, 1H), 7.93 – 6.76 (m, 62H), 6.72 (s, 1H), 6.45 (s, 1H), 6.42 (s, 1H), 6.32 (d, 1H), 6.25 (s, 1H), 6.20 (s, 1H), 6.17 (s, 1H), 5.94 (s, 1H), 5.90 (s, 1H), 5.83 (s, 1H), 5.80 (m, 2H), 5.79 (s, 1H), 5.78 (s, 1H), 5.76 (s, 1H), 5.74 (s, 2H), 4.00 – 3.45 (m, 34H), 3.02 (m, 1H), 2.86 (s, 3H), 2.39 – 2.11 (m, 17H), 2.06 (t, 2H), 1.72 – 1.61 (m, 2H), 1.42 – 0.82 (m, 118H). MS (ES^+): *m/z* calcd for $C_{270}H_{279}N_{34}O_{36}S$ $[M+2H]^{2+}$ 2304.55, found 2304.54.

2.2.2.4 Synthesis of 4b

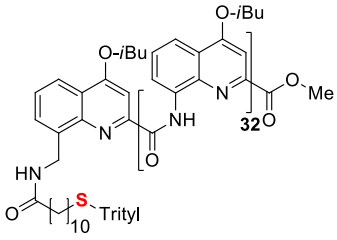

4a (100 mg, 0.012 mmol) was stirred with 50 % TFA in $CHCl_3$ (3 mL) at room temperature around 3h. After that TFA was removed by azeotrope with toluene on rotary evaporator. Then crude amine was re-dissolved in dry $CHCl_3$ (2 mL). Trityl protected mercaptoundecanoic acid (14 mg, 0.031 mmol), PyBOP (16 mg, 0.031 mmol) and DIPEA (0.009 mL, 0.062 mmol) were added and the reaction mixture was stirred at 40 °C overnight. End product was purified by precipitated in MeOH to obtain **4b** as a light yellow coloured solid (100 mg, 95%). ^{1}H NMR (300 MHz, $CDCl_3$): δ 11.07 (s, 1H), 11.02 (s, 1H), 10.70 (s, 1H), 10.64 (s, 1H), 10.43 (s, 1H), 10.21 (s, 1H), 10.18 (s, 1H), 10.11 (s, 1H), 10.04 (s, 1H), 9.98 (s, 1H), 9.92 (s, 1H), 9.84 (m, 2H), 9.77 (s, 1H), 9.72 (s, 1H), 9.66 (s, 2H), 9.61 (s, 2H), 9.56 (s, 2H), 9.53 (s, 2H), 9.48 (m, 9H), 7.91 (d, 1H), 7.85 (d, 1H), 7.80 (d, 2H), 7.67 – 6.53 (m, 112H), 6.38 (s, 1H), 6.35 (s, 1H), 6.26 (d, 1H), 6.19 (s, 1H), 6.11 (s, 1H), 6.08 (s, 1H), 5.84 (s, 1H), 5.79 (s, 1H), 5.74 (s, 1H), 5.69 (s, 1H), 5.67 (s, 1H), 5.64 (s, 2H), 5.60 (s, 1H), 5.54 (m, 4H), 5.49 – 5.43 (m, 15 H), 3.87 – 3.30 (m, 34H), 2.31 – 2.01 (m, 33H), 1.35 – 0.79 (m, 214H). MS (ES$^+$): *m/z* calcd for $C_{494}H_{503}N_{66}O_{68}S$ $[M+3H]^{3+}$ 2828.60, found 2828.61.

2.2.3 General procedure of syntheses of compound 1c, 2c, 3c and 4c

Compound **1b** (**2b**, **3b** and **4b**) was dissolved in THF/MeOH (9:1 vol/vol). NaOH (20 equiv.) was then added into the solution. This mixture was stirred at room temperature and monitored by TLC until the reaction is complete. 0.1 M HCl was put to neutralize the base and protonate the resulting product. After removal of organic solvents, the residue was dissolved in $CHCl_3$, washed with water and brine, and dried with Na_2SO_4, filtrated and concentrated to yield the acid **1c** (**2c**, **3c** and **4c**) as yellowish solid.

2.2.3.1 Synthesis of 1c

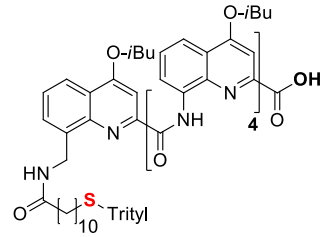

1b (170 mg, 0.125 mmol) was dissolved in 2-3 mL of THF/MeOH (9:1) and NaOH (50 mg, 1.25 mmol) powder was added. The reaction mixture was stirred at room temperature for 3 hours, then neutralized with 5% citric acid solution. The solvents were evaporated and dissolved in $CHCl_3$ and washed with water. The organic phase was dried over anhydrous Na_2SO_4 to get pure **1c** light yellow colored solid (160 mg, 95%). ^{1}H NMR (300 MHz, $CDCl_3$): δ 11.75 (s, 1H), 11.63 (s, 1H), 11.45 (s, 1H), 11.18 (s, 1H), 8.47 (dt, 2H), 8.19 – 8.11 (m, 2H), 8.04 – 7.90 (m, 5H), 7.59 (m, 2H), 7.45 – 7.19 (m, 21H), 6.87 (s, 1H), 6.74 (d, 1H), 6.68 (s, 1H), 6.65 (s, 1H), 4.74 (m, 1H), 4.37 – 3.81 (m, 11H), 3.61 – 3.54 (m, 1H), 2.61 – 2.27 (m, 5H), 2.13 (t, 2H), 1.69 – 1.64 (m, 2H), 1.39 – 1.01 (m, 46H). ^{13}C-NMR ($CDCl_3$, 75 MHz): 172.47, 163.51, 163.39, 163.24, 163.04, 162.28, 161.64, 161.50, 160.72, 160.56, 150.51, 150.44, 150.00, 148.38, 145.11, 144.64, 137.97, 137.69, 137.61, 137.12, 135.69, 133.50, 133.30, 133.12, 129.62, 127.80, 127.69, 127.49, 127.11, 126.85, 126.80, 126.50, 125.90, 122.58, 122.33, 122.20, 121.99, 121.81, 121.30, 117.91, 117.50, 116.88, 116.33, 116.12, 115.99, 115.75, 99.34, 98.78, 98.71, 98.60, 97.81, 77.30, 75.51, 75.18, 66.37, 38.76, 36.33, 32.02, 29.72, 29.31, 29.25, 29.17, 29.12, 29.00, 28.59, 28.27, 28.22, 28.20, 28.16, 28.11, 25.41, 19.45, 19.32, 19.20. MS (ES$^+$): *m/z* calcd for $C_{101}H_{109}N_{10}O_{12}S$ $[M+H]^+$ 1686.81, found 1686.80.

2.2.3.2 Synthesis of 2c

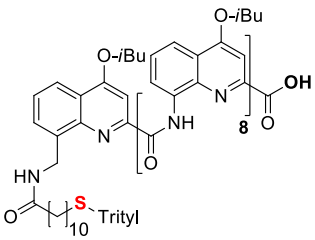

2b (150 mg, 0.056 mmol) was dissolved in 2 mL of THF/MeOH (9:1) and NaOH (22 mg, 0.56 mmol) powder was added. The reaction mixture was stirred at room temperature for 3 hours, then neutralized with 5% citric acid solution. The solvents were evaporated and dissolved in $CHCl_3$ and washed with water. The organic phase was dried over anhydrous Na_2SO_4 to get pure **2c** as a light yellow coloured solid (140 mg, 94%). ^{1}H NMR (300 MHz, $CDCl_3$): δ 11.26 (s, 1H), 11.18 (s, 1H), 11.01 (s, 1H), 10.94 (s, 1H), 10.89 (s, 1H), 10.85 (s, 1H), 10.78 (s, 1H), 10.75 (s, 1H), 8.24 – 8.15 (m, 4H), 8.03, (d, 1H), 7.98 – 7.80 (m, 8H), 7.69 (d, 1H), 7.58 (d, 1H), 7.46 – 6.99 (m, 27H), 6.96 (s, 1H), 6.87 (s, 1H), 6.82 (s, 1H), 6.63 (s, 1H), 6.50 (s, 2H), 6.47 (d, 1H), 6.37 (s, 1H), 6.22 (s, 1H), 6.07 (s, 1H),

4.19 – 3.76 (m, 18H), 3.24 (dd, 1H), 2.57 – 2.17 (m, 9H), 1.89 (t, 2H), 1.50 (m, 2H), 1.41 – 0.89 (m, 70H). ^{13}C-NMR ($CDCl_3$, 75 MHz): 172.39, 163.10 ,162.89, 162.85, 162.64, 162.61, 162.57, 162.39, 162.21, 162.05, 161.29, 161.05, 160.59, 160.17, 159.16, 159.03, 158.88, 158.50, 149.80, 149.65, 149.52, 148.96, 148.83, 148.53, 148.39, 148.04, 145.10, 144.13, 144.10, 137.60, 137.46, 137.29, 137.19, 137.09, 136.85, 135.37, 133.52, 133.34, 132.96, 132.79, 132.54, 132.50, 132.33, 132.12, 10.61, 127.78, 126.80, 126.67, 126.60, 126.49, 125.86, 125.59, 125.40, 122.31, 122.20, 122.10, 122.00, 121.89, 121.79, 121.73, 121.70, 121.35, 117.48, 117.15, 117.00, 116.94, 116.62, 116.47, 116.34, 116.23, 116.06, 115.94, 115.61, 115.51, 99.29, 98.80, 98.57, 98.47, 98.33, 97.45, 77.39, 75.33, 75.27, 75.12, 74.85, 67.94, 66.35, 38.47, 36.14, 31.99, 29.71, 29.39, 29.27, 29.18, 29.11, 29.07, 29.02, 28.97, 28.57, 28.16, 28.11, 28.04, 28.01, 27.96, 25.61, 25.34, 19.60, 19.55, 19.49, 19.45, 19.36, 19.33, 19.28, 19.23, 19.22, 19.15, 19.11. MS (ES^+): *m/z* calcd for $C_{157}H_{165}N_{18}O_{20}S$ $[M+2H]^{2+}$ 1328.12, found 1328.11.

2.2.3.3 Synthesis of 3c

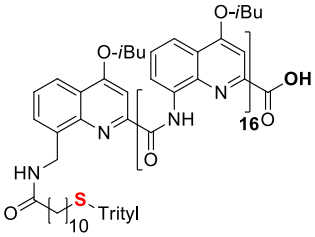

3b (41 mg, 0.009 mmol) was dissolved in 2 mL of THF/MeOH (9:1) and NaOH (7 mg, 0.177 mmol) powder was added. The reaction mixture was stirred at room temperature for 3 hours, then neutralized with 5% citric acid solution. The solvents were evaporated and dissolved in $CHCl_3$ and washed with water. The organic phase was dried over anhydrous Na_2SO_4 to get a pure 3c as a light yellow coloured solid (35 mg, 85 %). ^{1}H NMR (300 MHz, $CDCl_3$): δ 10.91 (s, 1H), 10.78 (s, 1H), 10.71 (s, 1H), 10.53 (s, 1H), 10.51 (s, 1H), 10.33 (s, 1H), 10.27 (s, 1H), 10.22 (s, 1H), 10.19 (s, 1H), 10.11 (s, 1H), 10.07 (s, 1H), 10.02 (s, 1H), 10.02 (s, 1H), 10.01 (s, 1H), 9.98 (s, 1H), 9.95 (s, 1H), 9.94 (s, 1H), 8.00 (t, 2H), 7.88 –7.64 (m, 19H), 7.40 – 6.75 (m, 46H), 6.71 (s, 1H), 6.56 (s, 1H), 6.45 (s, 1H), 6.34 – 6.31 (m, 2H), 6.13 (s, 1H), 6.11 (s, 1H), 5.92 (s, 1H), 5.89 (s, 1H), 5.82 (s, 1H), 5.81 (s, 1H), 5.78 (s, 2H), 5.77 (s, 1H), 5.75 (s, 1H), 5.73 (s, 2H), 4.00 – 3.44 (m, 34H), 3.01 (dd, 1H), 2.41 – 2.14 (m, 17H), 2.06 (t, 2H), 1.34 (t, 2H), 1.29 – 0.82 (m, 118H). MS (ES^+): *m/z* calcd for $C_{269}H_{277}N_{34}O_{36}S$ $[M+2H]^{2+}$ 2297.55, found 2297.54.

2.2.3.4 Synthesis of 4c

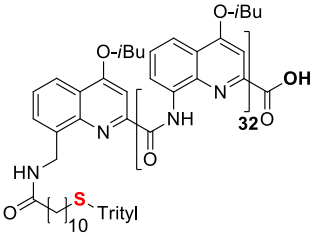

4b (100 mg, 0.012 mmol) was dissolved in 3 mL of THF/MeOH (9:1) and NaOH (38 mg, 0.942 mmol) powder was added. The reaction mixture was stirred at room temperature for 4 hours, then neutralized with 5% citric acid solution. The solvents were evaporated and dissolved in $CHCl_3$ and washed with water. The organic phase was dried over anhydrous Na_2SO_4 to get pure **4c** as a light yellow coloured solid (96 mg, 96 %). ^{1}H NMR (300 MHz, CDCl3): δ 10.84 (s, 1H), 10.70 (s, 1H), 10.64 (s, 1H), 10.48 (s, 1H), 10.43 (s, 1H), 10.24 (s, 1H), 10.18 (s, 1H), 10.11 (s, 1H), 10.07 (s, 1H), 9.98 (s, 1H), 9.94 (s, 1H), 9.84 (s, 2H), 9.77 (s, 1H), 9.73 (s, 1H), 9.66 (s, 2H), 9.61 (s, 2H), 9.56 (s, 2H), 9.48 (m, 11H), 7.99 – 6.53 (m, 118H), 6.42 (s, 1H), 6.31 (s, 1H), 6.26 (d, 1H), 6.05 (s, 2H), 5.84 (s, 1H), 5.79 (s, 1H), 5.74 (s, 1H), 5.70 (s, 1H), 5.67 (s, 1H), 5.65 (s, 2H), 5.61 (s, 1H), 5.54 (s, 4H), 5.49 – 5.44 (m, 14H), 3.91 – 3.30 (m, 34H), 2.96 (m, 1H), 2.28 – 2.01 (m, 33H), 1.33 – 0.79 (m, 218H). MS (ES^+): *m/z* calcd for $C_{493}H_{501}N_{66}O_{68}S$ $[M+3H]^{3+}$ 2823.93, found 2823.93.

2.2.4 General procedure of syntheses of compound 1d, 2d, 3d and 4d

Dry **1c** (or **2c**, **3c**, **4c**) (1 equv.), PEG (1.5 equv.) and PyBOP (2 equv.) were added to a flask and dissolved in anhydrous $CHCl_3$ under argon. Freshly distilled DIPEA was put into the flask dropwise. The reaction was allowed to process overnight and monitored by HNMR. After **1c** (or **2c**, **3c**, **4c**) was consumed completely, the resulting crude was purified by bio-bead column firstly and then recycling GPC, yielding the product **1d** (or **2d**, **3d**, **4d**).

2.2.4.1 Synthesis of 1d

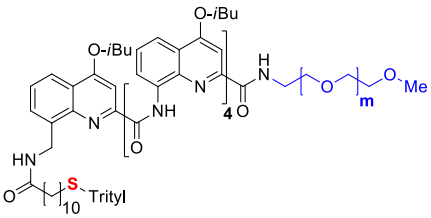

130 mg **1c** (113.3 μmol), 687 mg PEG (136 μmol) and 118 mg PyBOP (227 μmol) were dissolved in $CHCl_3$, and then 74.6 μL DiPEA was added dropwise into the mixture. After reacted at room temperature overnight, the reaction crude was purified by bio-bead column and recycling GPC, generating **1d**. ^{1}H NMR ($CDCl_3$, 300 MHz) δ ppm: 11.90 (1H, s), 11.75 (1H, s), 11.56 (1H, s), 11.54 (1H, s), 8.51 (2H, t), 8.18 – 8.07 (4H, m), 8.01 (1H, s), 7.99 (1H, s), 7.90 (1H, d), 7.79 (1H, d), 7.70 – 7.60 (4H, m), 7.42 – 7.17 (, m), 6.84 (1H, s), 6.71 (1H, s), 6.65 (1H, d), 6.61 (1H, s), 4.40 – 0.81 (belong to PEG and the side chains of quinoline). MS (ES^+): *m/z* calcd for $C_{100}H_{105}N_{10}O_{11}S$-NH-$(CH_2CH_2O)_{128}$-Me $[M+5H]^{5+}$ 1467.45, found 1467.87.

2.2.4.2 Synthesis of 2d

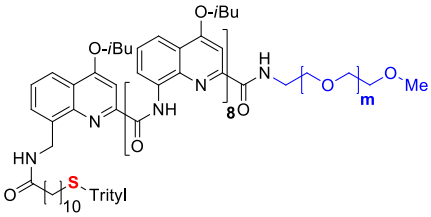

113 mg 2c (42.6 μmol), 258 mg PEG (51 μmol) and 44 mg PyBOP (85 μmol) were dissolved in $CHCl_3$ under argon, and then 28 μL DiPEA was added dropwise into the mixture. After overnight, the reaction crude was purified by bio-bead column and recycling GPC, generating **2d**. 1H NMR (CDCl3, 300 MHz) δ ppm: 11.42 (1H, s), 11.14 (1H, s), 11.06 (1H, s), 10.95 (1H, s), 10.82 (1H, s), 10.81 (1H, s), 10.77 (1H, s), 10.70 (1H, s), 8.15 – 8.08 (3H, m), 8.02 (1H, s), 7.99 (1H, s), 7.84 – 7.69 (4H, m), 7.63 (1H, d), 7.53 (1H, d), 7.41 – 6.82 (,m), 6.60 (1H, s), 6.54 (1H, s), 6.48 (1H, s), 6.44 – 6.41 (2H, d), 6.40 (1H, s), 6.16 (1H, s), 6.02 (1H, s), 4.17 – 0.87 (belong to PEG and the side chains of quinoline). MS (ES^+): *m/z* calcd for $C_{156}H_{161}N_{18}O_{19}S$-NH-$(CH_2CH_2O)_{118}$-Me $[M+5H]^{5+}$ 1573.48 found 1573.50.

2.2.4.3 Synthesis of 3d

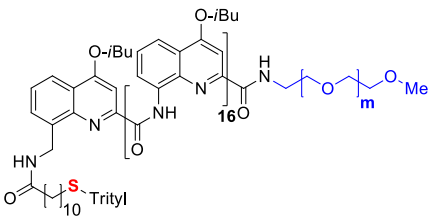

Dry **3c** (24 mg, 5 μmol), PEG (30 mg, 6 μmol) and PyBOP (5 mg, 10 μmol) were mixed and dissolved in 1 mL $CHCl_3$. 44 μL DiPEA (25 μmol) was added into the mixture dropwise. After the reaction was finished, the crude was purified by recycling GPC, yielding the target product **3d**. ^{1}H NMR ($CDCl_3$, 300 MHz) δ ppm: 11.08 (1H, s), 10.81 (1H, s), 10.73 (1H, s), 10.67 (1H, s), 10.41 (1H, s), 10.25 (1H, s), 10.23 (1H, s), 10.17 (1H, s), 10.12 (1H, s), 10.07 (1H, s), 10.03 (1H, s), 9.98 (1H, s), 9.97 (1H, s), 9.94 (1H, s), 9.90 (2H, s), 7.87 – 7.53 (24H, m), 7.36 – 6.67 (H, m), 6.38 (1H, s), 6.36 (1H, s), 6.26 (2H, s), 6.17 (1H, s), 6.12 (1H, s), 5.89 (1H, s), 5.85 (1H, s), 5.78 (1H, s), 5.75 (2H, s), 5.74 (1H, s), 5.73 (1H, s), 5.70 (1H, s), 5.69 (2H, s), 3.87 – 0.85 (belong to PEG and the side chains of quinoline). MS (ES^+): *m/z* calcd for $C_{268}H_{273}N_{34}O_{35}S$-NH-$(CH_2CH_2O)_{128}$-Me $[M+6H]^{6+}$ 1706.25 found 1709.05.

2.2.4.4 Synthesis of 4d

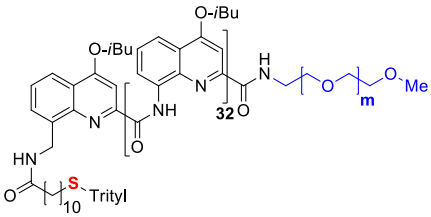

85 mg **4c** (10.5 μmol), 80 mg PEG (15.8 μmol) and 11 mg PyBOP (21 μmol) were dissolved in 1.5 mL $CHCl_3$, and then 90 μL DiPEA was added dropwise into the mixture. After overnight, the reaction crude was purified by bio-bead column and recycling GPC, generating **4d**. ^{1}H NMR ($CDCl_3$, 300 MHz) δ ppm: 11.00 (1H, s), 10.74 (1H, s), 10.64 (1H, s), 10.59 (1H, s), 10.31 (1H, s), 10.14 (2H, d), 10.05 (1H, s), 9.99 (1H, s), 9.92 (1H, s), 9.87 (1H, s), 9.80 (1H, s), 9.78 (1H, s), 9.71 (1H, s), 9.66 (1H, s), 9.61 (2H, s), 9.55 – 9.43 (15H, m), 7.79 – 6.47 (H, m), 6.31 (1H, s), 6.28 (1H, s), 6.20 (2H, d), 6.08 (1H, s), 6.02 (1H, s), 5.78 (1H, s), 5.73 (1H, s), 5.69 (1H, s), 5.62 (1H, s), 5.61 (1H, s), 5.59 (2H, s), 5.54 (1H, s), 5.49 – 5.37 (18, m), 3.87 – 0.81 (belong to PEG and the side chains of quinoline). MS (ES^+): *m/z* calcd for $C_{492}H_{497}N_{66}O_{67}S$-NH-$(CH_2CH_2O)_{100}$-Me $[M+6H]^{6+}$ 2146.58 found 2143.96.

2.2.5 General procedure of synthesis of compound 1e, 2e, 3e and 4e

The deprotection reaction was carried out via following the classic method.[1] The related compound **1d** (or **2d**, **3d**, **4d**) was added into a mixture (0.9 mL TFA, 0.05 mL $CHCl_3$ and 0.05 mL H_2O). The deprotection was allowed to react for 2 h. Afterward, TFA and H_2O were azeotroped by toluene under reduced pressure for ~ 4 times. The resulting solid was used without further purification to prepare the solution which allowed the resultant product (**1e, 2e, 3e and 4e**) to graft onto the Au surface

2.3 Immobilization of the helices on Au/Si substrates

The molecules were grafted onto gold-coated silicon substrates (Au (100nm) / Ti / Si wafer, Sigma-Aldrich) using our previously established method[2] to obtain a sparse regime of the molecule of interest. Substrates were cut (2 × 2 cm^2), cleaned in a 1:1:5 volume ratio of NH_4OH, H_2O_2, and H_2O solution during 15 min at 65°C, followed by UV-ozone treatment for 15 min (UV-ozone cleaner®, Model 42, Jelight Company Inc.) and finally dipped in EtOH for 5 min. Just after the cleaning procedure, they were dried by a N_2 flow and dipped for 1 h at room temperature in a solution of the helices ($4 \cdot 10^{-8}$ mol) and dodecyl sulfide (DDS) ($1 \cdot 10^{-7}$ mol) in dichloromethane. The functionalized substrate was then rinsed three times in filtered dichloromethane and finally dried with N_2 flow.

2.4 AFM force experiments

Experiments were carried out with a PicoPlus 5500 microscope (Agilent Technologies) equipped with a closed-loop scanner. Gold-coated tips (OBL-10 Biolever, Bruker; nominal spring constant k = 0.009–0.1 $N \cdot m^{-1}$ and k = 0.002-0.02 $N \cdot m^{-1}$) were used for all the force experiments. The spring constant of each cantilever was calibrated by the thermal noise and Sader methods[3,4]. Practically, before each experiment, we calibrate the cantilevers in air by the thermal noise method and after the experiment, we systematically use the Sader method, measure the cantilever dimensions by scanning electron microscopy and use the resonance frequency *f* and quality factor *Q* to obtain the spring constant value. We only considered experiments for which the spring constant values obtained by both methods were consistent. We also recorded the thermal fluctuation spectrum in liquid. We obtained a *Q* factor of 1.9, a resonance frequency *f* of 8.9 kHz and a response time of 68 µs in liquid. However, while the response time of a cantilever may be derived from the resonance frequency and *Q* factor from the thermal spectrum, the actual response time at the point of measurement can vary to a great extent from this value, especially when the cantilever is near the surface and/or under tension by the molecule[5,6]. The actual response time has been estimated by fitting an exponential decay to the force-time response after a force step in a force curve[6,7]. The response time during our experiments was estimated at 5 µs (Figure S14), thus short enough to observe the refolding events reported.

Before starting the experiments, the cantilever was immersed during 1 h in the solution of measurement for equilibration, away from the surface.

Force measurements were performed at pulling rates between 30 $nm \cdot s^{-1}$ (nominal loading rate of 1×10^3 $pN \cdot s^{-1}$) and 4200 $nm \cdot s^{-1}$ (nominal loading rate of 1.25×10^5 $pN \cdot s^{-1}$) in DMF, which correspond to sampling rates of 600 and 300.000 points per second, respectively. The molecules were picked up by gently pressing the AFM tip with a maximum force of 250 pN against the substrate.

When a molecule attaches to the tip during the approach, one can follow its stretching in the retraction curve by observing the cantilever deflection. The 'deflection *versus* z-movement' curves obtained were transformed into 'force *versus* distance' curves using the deflection sensitivity measured on each curve and the Hooke's law as

$$F = k\,\Delta x \text{ and } d = Z - \Delta x$$

with *F* the force experienced by the molecule, *k* the cantilever spring constant, Δx the deflection of the cantilever, *d* the distance between the tip and the substrate, and *Z* the vertical piezo-displacement.

2.5 Data analysis

The Force-Distance curve analyses were performed with IgorPro (WaveMetrics) using customized routines. The selection of the Force-Distance curves was done manually in order to identity and categorized the different patterns.

For each curve, we measured the length and force of the plateau. The force is measured at the middle of the plateau. Histograms of lengths and forces were constructed. We used a bin of 5 pN for the histograms of forces and a bin of 0.5 nm for histograms of lengths. The possible presence of multi-modal distributions was checked by using a probability density function (pdf) and a Gaussian mixture model (GMM) in MatLab. The distributions were fitted with Gaussian functions $G(\boldsymbol{x}|\mu_i, \sigma_i)$ with mean μ_i and variance σ_i, to determine the most probable values.

For each estimated average rupture force or length, the 95% confidence interval was computed as $1.96\sqrt{\sigma^2/(p_i N)}$ where σ^2 is the estimated variance of the i^{th} Gaussian component while $p_i N$ represents the effective size of the population.

2.6 Theoretical unwound structures and lengths

From the X-Ray structure of n 8-mer of 8-amino-2-quinolinecarboxylic acid,[8] all possible bond-rotations were mechanically tested. Molecular Models calculation were done using MacroModel version 8.6 (Schrödinger Inc.). Energy minimized structures were initiated from manually pre-organized structures, using MMFs force-field as implemented in this software, 500 steps of Truncated Newton Conjugate Gradient (TNCG), no implicit solvent and the extended Cutoff option. The best match between the length of theoretical structure and of the experimental unwound structure is obtained with the most extended, which is achieved through the rotation of each Cα−CO bonds of around 180°.
The theoretical difference in length between the unfolded and folded structures was obtained by subtracting the X-Ray folded length to the theoretical unfolded length obtained by the MMFs force-field calculations (Table S1). The length of the unwinding plateau observed experimentally nicely agrees with the expected difference in length between the unfolded and folded structures.

2.7 Analysis of the hopping states

Q33 was pulled at various loading rates, between 1,000 pN·s^{-1} (33 nm·s^{-1}) and 125,000 pN·s^{-1} (4200 nm·s^{-1}), and the hopping was further analysed. The hopping events occur especially at the end of the plateau (force around 100 pN) and up to a loading rate of 125,000 pN·s^{-1} (4200 nm·s^{-1}). The determination of the fluctuation rate at 100 pN was performed manually. We measured the total time over which these fluctuations occur (Δt_F), and we determined the number of fluctuations between folded and unfolded states during Δt_F. By averaging the number of fluctuations per time unit over hundred curves, we obtained the fluctuation rate.

For each fluctuation, we determined the duration of the transition from the unfolded state to the partially folded state. The average value over all the fluctuations corresponds to the rewinding rate under an external force of 100 pN.

2.8 Pulling-Relaxing experiments

For pulling-relaxing experiments, before and after every cycle, a few curves in which none molecule has been stretched have been selected as references. From the comparison between these measurements possible drift could be identified. The baseline of the curve before the cycle is used as the zero force value for the first curve of the cycle; the stretching profiles of the successive curves are superimposed and the consistency of the proposed zero force value is tested on the last curve of the cycle, when the molecule is lost and the force drops to zero. The zero extension is the reference position of the piezo (contact point) evidenced by the change in the slope of the force extension curve that becomes vertical. The zero extension during the cycle was easily identified thanks to the presence of the partial contact line or we used the same procedure used to identify the zero force: the zero length position identified in the last curve before the cycle is assigned to the first curve of the cycle, the stretching profiles of the curves of the cycle are superimposed and the consistency of the proposed position of the zero length is tested in the first curve after the cycle.

We measured the free-energy of unwinding and rewinding by integrating the area between the 'force *vs* extension' curve (both pulling and relaxing traces) and a WLC fit accounting for the elastic contribution from the stretching of the molecule. We thus measured the area beneath the plateau, and from this area, we subtracted the elastic contribution from the molecule stretching by adjusting a WLC fit on the last part of the curve. We followed the method described by Bustamante et al.[9] This method has been shown to be not very accurate when measuring the area of peaks in force curves.[10] Indeed, when a

domain of interactions ruptures and the cantilever snaps, the force on the molecule is not registered and, therefore, the free energy surface may not be recovered with high accuracy. However, here we measure the area under the plateau, outside the region of cantilever snap (Figure S15).

2.9 Transformation of force spectroscopy data from extension space into contour length space

Each experimental data of the Force-Distance curves was converted into contour length (L_c) value by solving numerically the worm-like chain (WLC) equation using MATLAB (MathWorks), as described in details in ref. (11). The WLC model predicts the relationship between the extension of an individual linear and flexible polymer chain and its entropic restoring force. The force required to extend a WLC with a persistence length l_p and contour length L to a distance D is given by:

$$F(D) = \frac{k_B T}{l_p}\left[\frac{D}{L} + \frac{1}{4(1-\frac{D}{L})^2} - \frac{1}{4}\right]$$

with k_B the Boltzmann constant and T the temperature. We used a l_p of 0.4 nm. The persistence length of PEO in DMF is 0.35 nm.[2,12] To take into account the contribution of the helix that will act as a rigid segment, we used a slightly higher value that perfectly fits the extension.[12]

These L_c values were plotted over time and exhibit stepwise increasing patterns. Histograms of the L_c values were constructed with a bin size of 0.15 and their distributions gave rise to multipeak histograms. We automatically fitted these histograms using Peakfit (Systat Software, Inc) and multiple Gaussian fit. Although the number of Gaussians obtained may seem quite arbitrary, especially for long helices, this is not the case. We systematically obtained a number of Gaussian peaks proportional to the length of the helix. For short helices (Q5 and Q9), the number of Gaussians is very restricted (2 for Q5 and 4 for Q9) and corresponds to a ratio of one Gaussian for 2 quinoline units. We also obtained the same ratio for the longer helices, which validates the fitting multipeak method.

For the cross-superposition graphs, we used MATLAB (MathWorks) to cross-superimposed the L_c values (including a standard deviation of 68% of the data of each peak) of two L_c distributions from two force-distance curves. Mathematically, we identified the successive matches between the intermediate states of each pulling curve and their intersection on the diagonal to highlight the similarities in the unwinding pathways of the two pulling experiments. The detailed procedure is described in ref. (6). Rectangles, representing each unfolding step, were drawn from the first possible match of the n L_c value and the last possible match of the n+1 L_c value, taking into account the L_c range.

The force curves used to build the 2D graphs have been randomly selected. We have analysed 20 curves for each foldamer, i.e. 80 curves in total. In about 20% of the cases, we identified a missing peak.

2.10 Anomalous Diffusion Object Motion Analysis (ADOMA)

The forces recorded *vs*. time in the single-molecule force spectroscopy experiments are analyzed as stochastic sequences. For a random process, x(t), the second moment or mean square displacement (MSD), is often considered as a good indicator to classify the motion as either normal/Brownian or anomalous. In equation (1),

$$< x^2(t) >= dt^{\gamma} \qquad (1)$$

”normality” is present if the left side of the process, $x(t)$, grows linearly in time, that is if $\gamma = 1$. In the following, the process is actually the force that is measured in the experiments, so its second moment is called MSF. For $0 < \gamma < 1$, the process is slower than “normal”, it explores the available “space of values” more slowly and is called sub-normal or sub-diffusive. For $1 < \gamma < 2$, the process is super-diffusive and explores the available “space of values” much faster than the previous ones.

In order to avoid biases introduced by the initial conditions, the original data is used to construct a set of several time series. In each of trajectory, every data-point contains the absolute value of the change

between two data-points of the initial series. A different, and increasing, distance between two measurements, also called time lag, characterizes every new time series. In practice, given an initial value, the difference is calculated with respect to a measurement that is further and further away, as the successive number that labels the series increases. The parameter *t* is the lag and its increase generates each series. The value of *t* is in the range 0<*t*<T/10, where T is the total length of the initial trajectory. The number of time series that are generated is therefore one tenths of the number of points present in the experiment.
It is crucial to emphasize that the lag does not refer to a delay with respect to the start or the end of the experiment, but to subsequent frames that move along the experiment.

Analysis of the MSF is often not sufficient to obtain information on the processes that govern the dynamics. The generalized moment method, GMM, can provide deeper insight. The method has found a variety of applications.[13-19] Details are found in ref. 16. GMM requires the calculation of several moments. The moments are calculated for each series. The first moment is the mean, the second moment is related to MSF and both first and second define the variance. The order of the moments can be non-integer (or even negative, although not here). Moments up to second order are responsible for the shape of the core of the probability distribution function, *pdf*, which is Gaussian for a Brownian process, while moments higher than two contribute to the tails of the *pdf*. If the process is Gaussian then the first two moments are enough to fully define the distribution.
In general, we expect that a stochastic process, to some extent, expresses self-similarity, and accordingly its moments, q, scale as

$$Q(t,q) \sim t^{z(q)} \tag{2}$$

The exponent *z*(*q*) in equation (2) is called “structure function” and contains the scaling exponents of each moment. Its form provides insights on the stochastic nature of a random/stochastic process.[15,16,21] Processes can be of a varying degree of complexity. When a process can be described by a unique scaling exponent, viz. monofractal process, then the structure function takes a simple form $z(q) = Hq$, see also below, and there is a direct relation between the exponent γ and the structure function coefficient *H*, namely, $\gamma = 2H$, where *H* is the Hurst exponent. The Hurst exponent is defined as the value of the structure function for *q*=1. In practice for a normal stochastic process, $H = 0.5$. We should notice that independently of the form/equation associated to the structure function, the coefficient of its linear term should take values close to the value of *z* at *q*=1. For *H*=0 the time series are stationary, while for *H*≠0 the resulted time series correspond to fractional integration of stationary increments. If *z*(*q*) shows a convex shape then the process is multifractal, multiple time scales exist and care is needed to classify the mechanisms generating randomness. Among multifractals, universal multifractals are ubiquitous and their structure function reads[20,21]

$$z(q) = Hq - \frac{C}{\alpha - 1}(q^{\alpha} - q) \tag{3}$$

where $C \geq 0$ indicates intermittency or the fractality of the process, the higher the value of *C* the stronger the intermittent effects, for *C*=0 the process is monofractal, α identifies the family of Levy α-stable distributions to which the probability distribution belongs to, and it provides information about the relative variation of intermittency around the mean. α=1 assigns the distribution to Cauchy-Lorentz which points to resonance effects, α=2 assigns the distribution to log-normal Kolmogorov pointing to the existence of a multiplicative mechanism result of at least two random processes.
In the present treatment, we consider moments of the recorded forces up to fourth order including also fractional ones, with a step of 0.5 for moments higher than 1, and with a step of 0.25 from 0.25 up to 1.

Analysis of the pulling/relaxing recorded forces at the plateau

The data were initially analyzed in terms of MSF of the forces (Figure 6 of the manuscript and Table S2 according to eq. (1)). The data of the plateau were also analyzed by means of GMM. As for the MSF, a unique description as function of the lag time is absent, instead, the same two different regimes are revealed, Figure S16. We fit each moment by a power law of the form at^b and the best obtained parameters (*a*, *b*) are listed in Table S3 for both pulling and relaxing. Notice that for q=2 the parameters (*a*, *b*) are the same with (*d*, *γ*) obtained for MSF by use of eq. (1).

We then estimated the structure function, see Figure 6 of the main text and Table S4 of the estimated parameters *H*, *C*, and α of eq.(3). There are two distinct regimes. In the first regime of short time lags, the structure function of both pulling and retracting has a convex form and draws steps from the Cauchy-Lorentz distribution. The second regime shows a remarkably different trend for pulling and retracting. A small non-linearity, with a *C* value of 0.004 is present for retracting.
Notice also that the Cauchy-Lorentz, also known as Lorenz in literature, distribution has the form $\mathrm{P}(\mathrm{x}, \mathrm{x}_0; \mathrm{b}) = \frac{1}{\pi} \frac{\mathrm{b}}{(\mathrm{x}-\mathrm{x}_0)^2+\mathrm{b}^2}$ where *b* is the scale parameter, and x_0 gives the maximum of the distribution, and for stochastic resonance would give the maximum force at resonance.

3 References

1. Méndez-Ardoy, A., Markandeya, N., Li, X., Tsai, Y.T., Pecastaings, G., Buffeteau, T., Maurizot, V., Muccioli, L., Castet, F., Huc, I., et al. (2017). Multi-dimensional charge transport in supramolecular helical foldamer assemblies. Chem. Sci. *8*, 7251–7257.
2. Lussis, P., Svaldo-Lanero, T., Bertocco, A., Fustin, C.-A., Leigh, D.A., and Duwez, A.-S. (2011). A single synthetic small molecule that generates force against a load. Nat. Nanotechnol. *6*, 553–557.
3. te Riet J., Katan, A.J., Rankl, C., Stahl, S.W., van Buul, A.M., Phang, I.Y., Gomez-Casado, A., Schön, P., Gerritsen, J.W., Cambi, A., et al. (2011) Interlaboratory round robin on cantilever calibration for AFM force spectroscopy. Ultramicroscopy *111*, 1659–1669.
4. Sader, J.E., Sanelli, J.A., Adamson, B.D., Monty, J.P., Wei, X., Crawford, S.A., Friend, J.R., Marusic, I., Mulvaney, P., and Bieske, E.J. (2012). Spring constant calibration of atomic force microscope cantilevers of arbitrary shape. Rev. Sci. Instrum. *83*, 103705.
5. Benmouna, F., and Johannsmann, D. (2002). Hydrodynamic interaction of AFM cantilevers with solid walls: An investigation based on AFM noise analysis. Eur. Phys. J. E *9*, 435–441.
6. Valotteau, C., Sumbul, F., and Rico, F. (2019). High-speed force spectroscopy: microsecond force measurements using ultrashort cantilevers. Biophys. Rev. *11,* 689–699.
7. Edwards, D.T., Faulk, J.K., Sanders, A.W., Bull, M.S., Walder, R., LeBlanc, M.-A., Sousa, M.C., and Perkins, T.T. (2015). Optimizing 1-μs-resolution single-molecule force spectroscopy on a commercial atomic force microscope. Nano Lett. *15,* 7091–7098.
8. Li, X., Qi, T., Srinivas, K., Massip, S., Maurizot, V., and Huc, I. (2016). Synthesis and Multibromination of Nanosized Helical Aromatic Amide Foldamers via Segment-Doubling Condensation. Org. Lett. *18*, 1044–1047.
9. Collin, C., Ritort, F., Jarzynski, C., Smith, S.B., Tinoco Jr, I., and Bustamante, C. (2005). Verification of the Crooks fluctuation theorem and recovery of RNA folding free energies. Nature *437*, 231–234.
10. Harris, N.C., Song, Y., and Kiang, C.-H. (2007). Experimental Free Energy Surface Reconstruction from Single-Molecule Force Spectroscopy using Jarzynski's Equality. Phys. Rev. Lett. *99*, 068101
11. Puchner, E.M., Franzen, G., Gautel, M., and Gaub, H.E. (2008). Comparing proteins by their unfolding pattern. Biophys J. *95*, 426–434.
12. Van Quaethem, A., Lussis, P., Leigh, D. A., Duwez, A.-S., and Fustin, C.-A. (2014). Probing the mobility of catenane rings in single molecules. Chem. Sci. *5*, 1449–1452.
13. Kolmogorov, A.N. (1940). Wienersche Spiralen und einige andere interessante Kurven im Hilbertschen Raum. Dokl. Acad. Sci. USSR *26*, 115–118.
14. Andersen, K.H., Castiglione, P., Mazzino, A., and Vulpiani, A. (2000). Simple stochastic models showing strong anomalous diffusion. Eur. Phys. J. B *18*, 447–452.
15. Seuront, L., and Stanley, H.E. (2014). Anomalous diffusion and multifractality enhance mating encounters in the ocean. Proc. Natl. Acad. Sci. U.S.A. *111*, 2206–2211.
16. Parent, L.R., Bakalis, E., Proetto M., Li, Y., Park, C., Zerbetto, F., and Gianneschi N.C. (2018). Tackling the Challenges of Dynamic Experiments Using Liquid-Cell Transmission Electron Microscopy. Acc. Chem. Res. *51*, 3–11.

17. Jeon, J.-H., Monne, H.M.-S., Javanainen, M., and Metzler, R. (2012). Anomalous Diffusion of Phospholipids and Cholesterols in a Lipid Bilayer and its Origins. Phys. Rev. Lett. *109*, 188103.

18. Bakalis, E., Hoefinger, S., Venturini, A., and Zerbetto, F. (2015). Crossover of two power laws in the anomalous diffusion of a two lipid membrane. J. Chem. Phys. *142*, 215102.

19. Parent, L.R., Bakalis, E., Ramirez-Hernandez, A., Kammeyer, J.K., Park C., de Pablo J., Zerbetto, F., Patterson, J.P., and Gianneschi, N.C. (2017). Directly Observing Micelle Fusion and Growth in Solution by Liquid-Cell Transmission Electron Microscopy. J. Am. Chem. Soc. *139*, 17140–17151.

20. Lovejoy, S., and Schertzer, D. (1995). Multifractals and rain. In New Uncertainty Concepts in Hydrology and Water Resources, Z.W. Kundzewicz, ed. (Cambridge University Press), pp. 61–103.

21. Bakalis, E., Parent, L.R., Vratsanos, M., Park, C., Gianneschi, N.C., and Zerbetto, F. (2020). Complex Nanoparticle Diffusional Motion in Liquid Cell Transmission Electron Microscopy. J. Phys. Chem. C *124*, 14881–14890.